ORIGIN AND THERMAL EVOLUTION OF MARS

G. Schubert[1], S. C. Solomon[2], D. L. Turcotte[3],
M. J. Drake[4] and N. H. Sleep[5]

Revised

February 5, 1990

[1]Dept. of Earth and Space Sciences and Institute of Geophysics and Planetary Physics (Paper No. 3253), University of California, Los Angeles, L. A., CA 90024. 213-825-4577. SPAN-5881::GSCHUBERT, BITNET-IAJ2GXS@UCLAMVS, NASAMAIL AND KOSMOS-GSCHUBERT. Communicating author.

[2]Dept. of Earth, Atmospheric, and Planetary Sciences, Massachusetts Institute of Technology, Cambridge, MA 02139. 617-253-3786.

[3]Dept. of Geological Sciences, Cornell University, Ithaca, NY 14850. 607-255-7282.

[4]Dept. of Planetary Sciences and Lunar and Planetary Laboratory, University of Arizona, Tucson, AZ 85721. 602-621-6952.

[5]Dept. of Geophysics, Stanford University, Stanford, CA 94305-2171. 415-723-0882.

ABSTRACT

The thermal evolution of Mars is governed by subsolidus mantle convection beneath a thick lithosphere. Models of the interior evolution are developed by parameterizing mantle convective heat transport in terms of mantle viscosity, the superadiabatic temperature rise across the mantle and mantle heat production. Geological, geophysical, and geochemical observations of the composition and structure of the interior and of the timing of major events in Martian evolution, such as global differentiation, atmospheric outgassing, and the formation of the hemispherical dichotomy and Tharsis, are used to constrain the model computations.

Isotope systematics of SNC meteorites suggest core formation essentially contemporaneously with the completion of accretion. Ancient fluvial landforms and a high atmospheric D/H ratio imply substantial degassing and atmosphere formation early in the history of Mars. Accretional considerations also favor initial melting of much of the outer portions of the planet. Initial conditions assumed for the thermal history calculations thus include full differentiation of silicate mantle and metal-sulfide core and a mantle at a high, near-solidus temperature.

The subsequent thermal evolution involves cooling of the mantle and core, differentiation of a crust, and thickening of a rigid lithosphere. As a result of the removal of much of the initial interior heat by vigorous mantle convection, perhaps augmented by an upward concentration of heat-producing elements into the crust, the rate of decrease of mantle temperature and surface heat flow was much more rapid during the first 1 Gyr of Martian history than subsequent to

that era. Crustal production rates were also much higher in the first 1 Gyr of Martian evolution than later in the planet's history. This temporal behavior is consistent with geological evidence for a general decrease with time in the Martian volcanic flux and, following a brief initial period of massive crustal formation, early global contraction recorded in the widespread formation of wrinkle ridges on geologically ancient surface units. The thermal evolution models predict a present lithosphere several hundred kilometers thick, in agreement with estimates of elastic lithosphere thickness inferred from the response to major surface loads.

Numerical calculations of fully three-dimensional, spherical convection in a shell the size of the Martian mantle are carried out to explore plausible patterns of Martian mantle convection and to relate convective features, such as plumes, to surface features, such as Tharsis. The models have upwellings in the form of cylindrical-like plumes and downwellings in the form of interconnected sheets. There is no single dominant plume. Therefore, if Tharsis is associated with one or more mantle plumes, then the lithosphere beneath Tharsis must be thinned or cracked either to promote plume concentration in the region or to facilitate magma migration through the lithosphere.

Thermal history models for Mars admit present core states similar to the Earth, but they also allow completely fluid cores and cores closer to complete freezing. The key parameter distinguishing among these possibilities is the weight fraction of sulfur in the core. If this fraction is about 15% or more, then the present Martian core is completely fluid and there is no thermal convective dynamo. The unambiguous determination of the presence or absence of an intrinsic

Martian magnetic field by future spacecraft missions will provide an essential constraint on interior structure and thermal evolution models. The eventual measurement of the natural magnetic remanence of rock samples on Mars with ages greater than 3.5 Gyr will also provide an essential test of thermal history and core dynamo models.

INTRODUCTION

The acceptance of Mars as the parent body of the SNC meteorites (McSween, 1984; Bogard et al., 1984; Becker and Pepin, 1984) has profoundly changed our view of the planet's evolution. Martian thermal history models of the late 1970s and early 1980s were largely dominated by the idea that the core of Mars formed subsequent to its accretion, after radioactive heating had raised the temperatures in the planet's interior sufficiently above the relatively cold initial temperatures to initiate melting and gravitational separation of Fe-FeS (Johnston et al., 1974; Solomon and Chaiken, 1976; Johnston and Toksöz, 1977; Toksöz and Johnston, 1977; Toksöz et al., 1978; Toksöz and Hsui, 1978; Solomon, 1978, 1979; Arvidson et al., 1980; Davies and Arvidson, 1981). Core formation in these models occurred as late as a few billion years after Mars accreted, and the segregation of the core lasted for up to a billion years. Late core formation was supported by the notion that Martian surface geology was dominated by extensional tectonics, requiring global heating and planetary expansion until late in the planet's evolution (Solomon and Chaiken, 1976; Solomon, 1978, 1979). However, the U/Pb isotopic composition of SNC meteorites requires core formation at about 4.6 Gyr ago (Chen and Wasserburg, 1986), either contemporaneous with accretion or within a few hundred million years of

the end of accretion. We must therefore abandon thermal evolution scenarios of Mars with cold initial temperatures and late core formation and instead adopt the view that accretional heating raised temperatures inside Mars sufficiently high that the core formed early, prior to the end of accretion or within a few hundred million years thereof, and that Mars began its post-accretional evolution fully differentiated and hot. In this new view of Martian thermal history early Mars was similar to the larger terrestrial planets Venus and Earth, whose cores formed early as a consequence of high accretional temperatures (e.g., Kaula, 1979*a*; Wetherill, 1985). The post-accretional evolution of Mars, like that of Venus and Earth, is one of secular cooling.

In the following, we will discuss the case for a hot initial Mars and early core formation in greater detail. Numerous lines of evidence, in addition to the U/Pb isotopic composition of SNC meteorites, support an early hot, differentiated planet. The structure of the Martian interior is a major factor in determining the post-accretional thermal history of Mars, and we briefly discuss interior structural models inferred from geophysical and geochemical data (see also chapter 2.3). In accordance with the model of early core and crust formation, we assume that the major radial structure of Mars has been little changed since the end of accretion (except for the lithosphere, which has thickened with time).

The principal characteristics of Mars, i.e., the north-south crustal dichotomy, the Tharsis Rise, the center of mass-center of figure offset, global tectonic patterns, and the possible absence of a magnetic field, must all be understood in terms of the thermal history,

and we discuss how these characteristics might be accommodated in a model in which Mars steadily cools from a hot, differentiated start. We present quantitative models of Martian cooling history that parameterize heat transport by subsolidus mantle convection. These models allow us to estimate properties of Mars for which no direct measurements presently exist, such as the cooling rate of the planet, its present lithosphere thickness and surface heat flux, and the present extent of inner core solidification. Finally, we use the results of numerical calculations of fully three-dimensional, spherical convection to discuss convective patterns in the Martian mantle. These computations place constraints on possible convective models for the formation of the hemispheric crustal asymmetry and Tharsis.

INTERNAL STRUCTURE

Though the seismic experiment on Viking Lander 2 provided no direct information on Mars' internal structure (Anderson et al., 1977; Goins and Lazarewicz, 1979; Toksöz, 1979), it is likely that Mars is divided into a crust, mantle and core. However, the thicknesses, densities and compositions of these regions are uncertain (see chapter 2.3).

Core

Geophysical and geochemical data constrain the size and composition of the Martian core. The geophysical data include the mean density of Mars (3933 kg m^{-3}, Bills and Ferrari, 1978) and its dimensionless axial moment of inertia, 0.365, according to Reasenberg (1977) and Kaula (1979*b*). The dimensionless axial moment of inertia C/MR^2, where C is the principal moment of inertia about the rotation axis, M is the mass of Mars, 6.42 x 10^{23} kg, and R is the radius of Mars, 3390 km, is

obtained from the inferred value of J_{2H} (the second-degree zonal coefficient in the spherical harmonic representation of the hydrostatic part of the gravitational potential of Mars). To determine C/MR^2 it is necessary first to remove the relatively large nonhydrostatic contribution J_2' to the observed J_2 ($J_2 = J_2' + J_{2H}$). Estimation of J_2' is model dependent and, as a result, the axial moment of inertia of Mars is uncertain. According to Reasenberg (1977) and Kaula (1979*b*), J_2' is principally due to Tharsis (see also Binder and Davis, 1973). Under the assumption that the nonhydrostatic contributions to the moments of inertia are symmetric about an equatorial axis through the center of Tharsis, it can be shown that $C/MR^2 = 0.365$ (Reasenberg, 1977; Kaula, 1979b), Bills (1989) has recently suggested that the nonhydrostatic component of J_2 is more likely to be a maximally triaxial ellipsoid, i.e., with the intermediate moment of inertia exactly midway between the greatest and least moments. This assumption leads to a value of C/MR^2 equal to 0.345. Kaula et al. (1989) have argued that the larger value of C/MR^2 is more physically plausible since : 1) the rotation axis of Mars adjusts sufficiently rapidly compared to changes in nonhydrostatic density anomalies that it is the axis of maximum moment of inertia for the nonhydrostatic density field, 2) the gravity and topography of Mars are dominated by Tharsis, and 3) tectonic models of Tharsis require generation and support that are almost axisymmetric about a line from the center of Mars through Tharsis.

Goettel (1981) has explored the consequences of the mean density and moment of inertia I of Mars for the radius of the Martian core and the densities of the planet's core and mantle ($I = (C+B+A)/3$, $I/MR^2 = C/MR^2 - 2J_2/3$, $J_2 = 1.96 \times 10^{-3}$). His results, based on

$I/MR^2 = 0.365$, are summarized in Table 1. (Spherically symmetric compositional models can only be constrained by I/MR^2 and other spherically averaged observables.) Mars could possess either a small, iron-rich core of high density (a pure Fe core would have a density of 8090 kg m^{-3} and constitute 14.8% of the mass of Mars), or a large, low-density core with substantial S (or other light element). An FeS core would have a density of 5770 kg m^{-3} and comprise 26.3% of the mass of Mars. The core mass increases with its size despite the density decrease (Figure 1). Goettel's (1981) results for core properties consistent with the mean density and the mean moment of inertia of Mars are in general agreement with the predictions of other models (Johnston and Toksöz, 1977; Okal and Anderson, 1978; Basaltic Volcanism Study Project, 1981). On the basis of all these models, the probable radius of the Martian core lies in the range 1500 to 2000 km, and the fractional mass of the planet occupied by the core is likely to be between 15 and 30 percent.

Independent geochemical evidence on the mass of the Martian core is provided by the SNC meteorites. Treiman et al. (1987) have determined the abundances of siderophile and chalcophile elements in the mantle of Mars from SNC meteorite abundances (using an element correlation method) and have modeled these abundances in terms of segregation of metal into the core. The abundances of siderophile and chalcophile elements may be substantially matched if Mars accreted homogeneously and a metallic core constituting 25-35 weight percent of the planet formed in chemical equilibrium with the mantle. Best fits are achieved if the core material during differentiation consisted of about 50% solid Fe-Ni metal and 50% liquid Fe-Ni metal containing about 25 weight percent S. The S content of such a core would be about 12.5 weight

percent. The ratio of Fe to Ni is poorly known, and the relative fractions of the solid and liquid components of both the early and modern core are unconstrained.

Laul et al. (1986) have also calculated the mass and composition of the core by assuming CI abundances of Fe and Ni and a 0.35 x CI abundance of S. From mass balance, and abundances of these elements inferred for the Martian mantle from the compositions of the SNC meteorites, they obtained a core comprising 21.7 weight percent of the planet, with a S abundance of 14 weight percent. Laul et al. (1986) also conclude that Mars accreted homogeneously and that the core is in equilibrium with the mantle. However, the low core mass that they compute does not yield as good a fit to the depletions of siderophile and chalcophile elements as the larger core masses of Treiman et al. (1987).

We will see in a later section that the abundance of S in the core of Mars is a crucial parameter determining the extent to which the core solidifies as the planet cools through geologic time. Unfortunately, the S content of the Martian core must still be considered as uncertain. The agreement between the estimates of Laul et al. (1986) and Treiman et al. (1987) of the weight percent S in the Martian core, while encouraging, may only reflect the use of the same limited geochemical data set by both groups.

Mantle

Consistent with the core properties summarized in Table 1, the thickness of the Martian mantle ranges between about 1500 and 2100 km. The zero pressure density of the mantle, for $I/MR^2 = 0.365$, is between about 3400 and 3470 kg m^{-3} (Goettel, 1981). If the olivine-spinel

phase transition occurs in the Martian mantle, it would be found at depths greater than approximately 1000 km (Basaltic Volcanism Study Project, 1981; chapter 2.3). Still higher pressure phase changes involving the formation of perovskite and magnesiowustite might occur in the deep lower mantle of Mars depending on the size of the Martian core (chapter 2.3).

Crust

Mars has a distinct low-density crust of variable thickness, as indicated by the partial to complete isostatic compensation of surface topography (Phillips et al., 1973; Phillips and Saunders, 1975). The mean thickness of the crust, however, is poorly constrained. A minimum value for the average crustal thickness of 28 ± 4 km (depending on choice of crust-mantle density difference) was obtained by Bills and Ferrari (1978) by fitting a model crust of uniform density and variable thickness overlying a uniform mantle to topography and gravity expressed in spherical harmonics to degree and order 10; for this minimum mean thickness the crust is of zero thickness beneath the Hellas basin. For a crustal thickness of 15 km at the site of the Viking 2 Lander seismic experiment, in agreement with the seismically inferred crustal thickness (Anderson et al., 1977), Bills and Ferrari (1978) obtained a mean crustal thickness of 37 ± 3 km. The crustal thickness beneath the Hellas basin in this model is 9 ± 1 km while beneath Tharsis it is 69 ± 8 km. In all the models of Bills and Ferrari (1978) maximum crustal thickness occurs beneath Tharsis and minimum crustal thickness is found beneath the Hellas basin. Sjogren and Wimberly (1981) used topography and gravity data to infer that the Hellas basin is isostatically compensated at a best-fitting

compensation depth of 130 ± 30 km. From the models of Bills and Ferrari (1978), this value corresponds to a globally averaged crustal thickness of about 150 km.

The approximately hemispherical division of the Martian surface between the topographically lower and stratigraphically younger northern plains and the heavily cratered southern uplands, often termed the crustal dichotomy, is associated with thicker crust in the southern hemisphere (e.g., Janle, 1983). The hemispheric crustal dichotomy contributes to the Martian center of mass-center of figure offset, as does the Tharsis bulge. The Martian center of figure is displaced from the center of mass by about 2.1 km in a direction toward 58°S, 94°W (Kobrick et al., 1981). This direction is approximately midway between the centers of the southern highlands and the Tharsis bulge (Roth et al., 1981).

CONSTRAINTS ON THERMAL EVOLUTION

Among the major constraints on thermal history models of Mars is the origin of the present internal structure of the planet. Viable thermal evolution models must account for the timing and formation of the core, the hemispheric crustal dichotomy, and the Tharsis Rise. Models should provide an explanation for the lack of a magnetic field at present, or, if future observations should prove the existence of a small Martian magnetic field, the models should allow for the generation of that field. Thermal history models should be consistent with the evolution of surface stresses and strains as revealed by global tectonic patterns.

Core Formation

U-Pb data for several SNC meteorites intercept the concordia curve at about 4.5 Gyr as well as at a younger age variously thought to represent the crystallization age of the shergottites (Jones, 1986) or the impact event that resulted in ejection of SNC material from the parent body (Chen and Wasserburg, 1986). The 4.5 Gyr "age" indicated by U-Pb data as well as whole-rock Rb-Sr model ages for SNC meteorites of about 4.6 Gyr (Shih et al., 1982) suggest early global differentiation, including formation of the core essentially contemporaneously with the completion of accretion. Differentiation of a core would heat Mars on average by as much as 300 K (Solomon, 1979). A hot initial state for the planet is indicated by these results. Other indicators of a hot early Mars include: (1) the old age (≥4 Gyr) of the southern hemisphere highlands, suggesting early crustal differentiation (see below), (2) geologic (ancient large flood features and valley networks, Carr, 1987) and isotopic (high atmospheric D/H ratio, Owen et al., 1988) evidence of early outgassing and an early atmosphere, and (3) tectonic evidence of global compression associated with planetary cooling over geologic time (see below).

Early core formation is made possible by the high accretional temperatures achieved through the burial of heat by large impacts (Kaula, 1979*a*; Wetherill, 1985). An example of accretional temperature profiles for Mars is shown in Figure 2 (Coradini et al., 1983). In this example there is a power-law distribution of impacting planetesimals by size, 30 percent of the impact kinetic energy is retained as heat, and a 100-Myr timescale of accretion is assumed. For this particular model, melting of a 360-km-thick shell occurs at the

end of accretion. Models with higher temperatures and larger degrees of melting are possible, for example by adoption of a larger value for the percent of impact kinetic energy retained as heat.

The importance of large impacts in the formation of the terrestrial planets and the validity of the 100 Myr accretional time scale are demonstrated by the planetary accumulation models of Wetherill (1985, 1986). The spin and orbital properties of Mars and the other planets, especially their obliquities, are plausibly explained as consequences of impacts with large bodies during the process of planetary formation (Harris and Ward, 1982; Hartmann and Vail, 1986). A major problem in understanding the growth of Mars according to present models of planetary accretion is that the calculations typically result in objects that are several times more massive than Mars (Wetherill, 1985, 1986). The size of Mars may have been limited by disturbances to the planetesimal source population for Mars associated with outer planet secular resonance regions, assuming of course that the formation of the outer planets preceded the growth of Mars (Wetherill, 1986).

Magnetic Field

Mars may have a small magnetic field, though this hypothesis is presently a matter of dispute (Russell et al., 1984; Dolginov, 1987). A fit of a dipole to the available Soviet magnetic field data gives a moment of 2×10^{22} Gauss-cm^3, or 3×10^{-4} times the Earth's moment, tilted about 15° with respect to the rotation axis and oriented in the opposite sense to the Earth's dipole moment (Dolginov et al., 1973, 1976). A re-evaluation by Russell (1978) leads only to an upper bound on the moment of 2×10^{21} Gauss-cm^3, an order of magnitude less than the value of Dolginov and co-workers. Recent Phobos observations of

the Martian magnetotail give no indication of an intrinsic planetary magnetic field (Riedler et al., 1989; Ong et al., 1989). Magnetic field measurements in the close vicinity of Mars are needed to resolve this issue.

Several SNC meteorites display natural remanent magnetization (NRM) consistent with a magnetizing field of less than about 0.1 oe (Cisowski, 1981, 1982). The timing and acquisition mechanism of the NRM are not well established, but it has been inferred that the magnetizing event was shock metamorphism during impact (Cisowski, 1982). Whether an internal magnetic field on Mars is indicated at the time the SNC meteorites were ejected from the planet is unclear.

Crustal Dichotomy

The relative chronology of the various large-scale surface units on Mars is reasonably well established from stratigraphic and crater density relationships (e.g., Carr et al., 1973; Tanaka et al., 1988; see chapters 3.1 and 3.2). The oldest units are the cratered terrain, an upland region as heavily cratered as the lunar highlands and occupying approximately the hemisphere south of a great circle inclined 35° to the equator (Mutch and Saunders, 1976). While the absolute chronology of the Martian surface is a matter of debate (e.g., Hartmann, 1973*a*, 1977; Soderblom et al., 1974; Neukum and Wise, 1976; Neukum and Hiller, 1981), most workers are in agreement that the heavily cratered southern uplands probably record the terminal phase of heavy bombardment of the inner solar system, dated for the Moon at 3.9-4.0 Gyr ago. The bulk of crustal formation must have occurred prior to this time.

The approximately hemispherical dichotomy between the ancient southern highlands and the younger northern plains is generally held to

be an ancient first-order feature of the Martian crust. The dichotomy as been ascribed variously to a very long-wavelength mantle convective planform (Lingenfelter and Schubert, 1973; Wise et al., 1979*b*), to post-accretional core formation (Davies and Arvidson, 1981), and to a giant impact (Wilhelms and Squyres, 1984). In view of the evidence from SNC meteorites, discussed above, that core separation occurred essentially contemporaneously with accretion, scenarios for the formation of the crustal dichotomy involving late core-mantle segregation (Wise et al., 1979*b*; Davies and Arvidson, 1981) may be discounted. Whether the dichotomy was the result of endogenic or exogenic processes, however, remains unresolved despite considerable ongoing photogeological analysis of the dichotomy boundary region (e.g., McGill, 1988; Wilhelms and Baldwin, 1988).

Volcanic Flux

Mars shows abundant evidence of surface volcanic activity spanning a wide range of relative geologic ages (see chapter 3.3). There are numerous volcanic constructs, including the large volcanoes of the Tharsis province, and extensive volcanic plains with apparent flow fronts and other features associated with volcanic units (Carr, 1973, 1974; Malin, 1977; Carr et al., 1977). There are relatively old and relatively young examples of both plains and shields. While the stratigraphic sequence of major volcanic units has been reasonably well established from crater density and superposition relationships (Tanaka et al., 1988), estimates of the absolute ages of volcanic units depend upon knowledge of the scaling of cratering flux and impacting-object size versus crater size from the Moon to Mars, knowledge that is, at best, incomplete (e.g., Chapman, 1974; Wetherill, 1974; Hartmann et al.

1981). Published ages for the stratigraphically young surfaces of the Tharsis shields, for instance, range from 2.5 Gyr (Neukum and Wise, 1976) to on the order of 0.1 Gyr (e.g., Hartmann, 1977).

An important constraint on global thermal evolution is the volcanic flux through time. Estimates of the surface area of volcanic material at each major stratigraphic stage, including corrections for later burial, have been given by Greeley (1987) and Tanaka et al. (1988). Both find 2 x 10^8 km^2 of volcanic material, though the two analyses differ in detail, particularly in the relative strength of a "peak" in the flux curve at early Hesperian times (corresponding to the formation of the Martian ridged plains) about 3 to 3.5 Gyr ago (Tanaka, 1986). In the more detailed synthesis of Tanaka et al. (1988) the early Hesperian "peak" is quite modest; a monotonic or nearly monotonic decrease of flux with time is implied. Greeley (1987) has suggested that the volume of volcanic material may be estimated by multiplying the area by an average thickness of about 1 km. A volume of 2 x 10^8 km^3 is equivalent to a global layer of volcanic material 1.5 km thick. Since the volume of igneous intrusions accompanying each eruption is generally larger than the volume of volcanic material (by a factor of 10 in continental regions on Earth (Crisp, 1984) and perhaps even larger on Mars), a significant fraction of the Martian crust may have been added by igneous activity since the end of heavy bombardment.

Global Tectonic Deformation

Large-scale patterns of tectonic deformation on a planetary surface can be direct signatures of global thermal evolution (see chapter 2.4). For a planet with a globally continuous lithosphere, such as Mars, warming or cooling of the interior will give rise to net global

expansion or contraction and thus, respectively, to extensional or compressional horizontal stress and strain near the planetary surface. The magnitude σ_t of thermal stress accumulated in any time interval is given by

$$\sigma_t = [E/(1-\nu)]\Delta R/R \qquad (1)$$

where E and ν are the Young's modulus and Poisson's ratio of near-surface material and $\Delta R/R$ is the fractional change in radius during that time interval (Solomon, 1986). The fractional radius change is related to the radial distribution of temperature change $\Delta T(r)$ by

$$\Delta R/R = (1/R^3)\int_0^R r^2 \alpha(r)\Delta T(r)dr \qquad (2)$$

where α is the volumetric coefficient of thermal expansion. For $\alpha = 3 \times 10^{-5}K^{-1}$, a change ΔT in average interior temperature of 100 K yields $\Delta R/R = 10^{-3}$ or $\Delta R = 3$ km. From (1), with E = 80 GPa and ν = 0.25, such a radius change corresponds to σ_t = 100 MPa(1 kbar). Sufficiently large thermal stress and strain should be visible in globally distributed tectonic features whose timing and sense of deformation yield strong constraints on the history of internal temperatures (e.g., Solomon and Chaiken, 1976). Large-scale tectonic features confined to a regional, rather than global, scale are also important indicators of thermal evolution, particularly of the characteristics of heat and strain imparted to the lithosphere by mantle dynamic processes.

The view of Martian tectonics that followed the Mariner 9 mission was that the planet experienced a prolonged period of lithospheric

extension which gave rise to the extensive systems of graben mostly centered on the Tharsis region (Hartmann, 1973*b*; Carr, 1974), the Valles Marineris canyon system (Sharp, 1973), and the pervasive volcanism (Carr, 1973). Thermal history models consistent with this view of tectonic evolution involved net warming and global expansion over much of Martian history. The net warming was attributed variously to late core formation (Solomon and Chaiken, 1976), to radioactive heating of the mantle following low-temperature differentiation of a sulfur-rich core (Toksöz and Hsui, 1978), or to degassing of the interior and a consequent "stiffening" of the mantle rheology (Tozer, 1985). As noted above, a hot initial state is now indicated for Mars from lead isotope data and planetary accretion considerations, so scenarios involving an initially cool interior (e.g., Solomon and Chaiken, 1976; Toksöz and Hsui, 1978) are not viable. Further, thermal history calculations explicitly including interior degassing and the consequent effect on mantle viscosity (McGovern and Schubert, 1990) do not show a secular warming of the mantle as suggested by Tozer (1985).

Much of the evidence for lithospheric extension on Mars is provided from tectonic features in and near the Tharsis area. Though the extensional fractures radiating from the center of Tharsis span a region more than 8000 km across, Tharsis may nonetheless be regarded as a regional feature rather than part of a response to global stress. Further, there are important compressional features located in the ridged plains of Tharsis and oriented approximately circumferential to the center of activity (Wise et al., 1979*a*). Considerable effort has gone into understanding the evolution of the Tharsis province from this regional perspective. The long-wavelength gravity and topography of

the region are not consistent with complete isostatic compensation by a single mechanism, such as crustal thickness variations (Phillips and Saunders, 1975). Complete local isostasy is possible, however, if a combination of Airy (crustal thickness variations) and Pratt (mantle density variations) mechanisms act in concert, but only if the crust is relatively thin (or is pervasively intruded by high-density plutonic material) beneath the Tharsis rise and substantial density anomalies persist to at least 500 km depth (Sleep and Phillips, 1979, 1985). Alternatively, a portion of the high topography of Tharsis can be supported by membrane stresses in the elastic lithosphere (Banerdt et al., 1982; Willemann and Turcotte, 1982).

These compensation models have been used to predict lithospheric stresses for comparison with the observed distribution of tectonic features. The isostatic model for Tharsis predicts stresses in approximate agreement with the distribution and orientation of extensional fractures in the central Tharsis region and of compressive wrinkle ridges, while the model involving lithospheric support of a topographic load predicts stresses consistent with the more distal extensional features in regions adjacent to the Tharsis rise (Banerdt et al., 1982; Sleep and Phillips, 1985). An evolution in the nature of the support of Tharsis topography has been suggested (Banerdt et al., 1982; Solomon and Head, 1982), though the sequence depends upon the relative ages of distal and proximal tectonic features. If the distal features are older, then viscoelastic relaxation of stresses associated with an early episode of lithospheric loading may have led to an essentially isostatic state at present; if the distal features are younger, then a progression from local isostasy to lithospheric support

as the Tharsis rise was constructed may have been the natural consequence of global interior cooling and lithospheric thickening (Sleep and Phillips, 1985). This distinction is complicated by the fact that superimposed global thermal stress is apparently required to account for the formation of many of the graben and wrinkle ridges, particularly in regions where both types of features are present.

Recent work on Martian tectonics may sharpen the constraints on global thermal stress. Chicarro et al. (1985) have utilized Viking images to map the global distribution of wrinkle ridges on Mars, including regions distant from Tharsis. They find that ridges occur commonly throughout ancient terrain. In volcanic plains, however, the distribution is highly uneven, with ridges strongly concentrated in the ridged plains units and in spotty occurrences in other regions. The lower Hesperian age (approximately 3 to 3.5 Gyr ago) for most major ridged plains units (Tanaka, 1986) and the contrast in ridge density between cratered uplands and young volcanic plains (Chicarro et al., 1985) suggest that ridge formation may have been concentrated in a comparatively early state in Martian evolution (Watters and Maxwell, 1986). Examination of crosscutting relations between ridges and graben also supports the view that most ridge formation in the Tharsis region was restricted to an early time period (Watters and Maxwell, 1983).

The Martian tectonic history most consistent with all of these findings is one in which Tharsis evolved after the end of heavy bombardment from a primarily isostatic state to one with long-term lithospheric support. Superimposed on the stresses associated with the Tharsis rise were a globally compressive stress produced by significant interior cooling in the interval 3 to 4 Gyr ago. Any additional cooling

(or warming) in the last 3 Gyr has been sufficiently modest so that further changes in planetary volume have not led to widespread development of young compressive (or extensional) features.

Lithospheric Thickness

Estimates of lithospheric thickness on Mars provide important constraints on near-surface thermal gradients and thus on heat flux. The thickness of the thermal lithosphere may be inferred approximately from the heights of volcanic constructs, and the thickness of the elastic lithosphere may be inferred from the response to volcanic loads.

Volcanic constructs on Mars show a tendency to increase in height with time of formation, in that the oldest such features are a few kilometers high and the youngest shields are approximately 20 km high with respect to surrounding terrain (Carr, 1974; Blasius and Cutts, 1976). This relation-ship has been ascribed to an increase in the hydrostatic head of the magma with time because of a progressive deepening of the source region (Vogt, 1974; Carr, 1976). Assuming a relative density contrast of 10% between magma and average overburden, and ignoring viscous head loss, these heights give depths to magma chambers varying from perhaps as little as a few tens of kilometers to somewhat over 200 km over the history of Martian shield formation.

The thickness T_e of the elastic lithosphere of Mars has been estimated from the tectonic response to individual loads (Thurber and Toksöz, 1978; Comer et al., 1985) and from the global response to the long-wavelength load of the Tharsis rise (Banerdt et al., 1982; Willemann and Turcotte, 1982). The spacing of graben circumferential to the major volcanoes Ascraeus Mons, Pavonis Mons, Arsia Mons, Alba

Patera and Elysium Mons indicate values for T_e of 20 to 50 km (equivalently, values of flexural rigidity D of 10^{30} to 10^{31} dyne cm) at the times of graben formation (Comer et al., 1985). For the Isidis basin region, the elastic lithosphere thickness is inferred to have exceeded 120 km ($D > 10^{32}$ dyn cm) at the time of mascon loading and graben formation (Comer et al., 1985). The absence of circumferential graben around Olympus Mons requires the elastic lithosphere to have been at least 150 km thick ($D > 3 \times 10^{32}$ dyn cm) at the time of loading (Thurber and Toksöz, 1978; Comer et al., 1985; Janle and Jannsen, 1986). Models of the response of Mars to the long-wavelength topography of the Tharsis rise provide a reasonable fit to the geoid and to the distribution of tectonic features in the Tharsis province if the elastic lithosphere of Mars is globally about 100 to 400 km thick, corresponding to $D=10^{32}$ to 7×10^{33} dyn cm (Banerdt et al., 1982; Willemann and Turcotte, 1982).

The values for T_e derived for individual loads are not consistent with a simple progressive increase with time in the thickness of the elastic lithosphere of Mars. The largest estimates of T_e, for instance, are for perhaps the oldest (Isidis mascon) and youngest (Olympus Mons) features considered (Tanaka et al., 1988). Spatial variations in elastic lithosphere thickness must have been at least as important as temporal variations (Comer et al., 1985). In particular, there appears to have been a dichotomy in lithosphere thickness that spanned a significant interval of time, with comparatively thin elastic lithosphere (T_e = 20 to 50 km) beneath the central regions of major volcanic provinces and substantially thicker elastic lithosphere (T_e in excess of 100 km) beneath regions more distant from volcanic province

centers and appropriate for the planet as a whole.

The values of T_e may be converted to estimates of the lithospheric thermal gradient and heat flow, given a representative strain rate and a flow law for ductile deformation of material in the lower lithosphere and estimates of lithospheric thermal conductivity. Under the assumption that the large values of elastic lithosphere thickness determined from the local response to the Isidis mascon and Olympus Mons and from the global response to the Tharsis rise exceed the thickness of the Martian crust, the depth to the base of the mechanical lithosphere is determined by the ductile strength of the mantle. The minimum values of T_e for the Isidis mascon and Olympus Mons correspond, by this line of reasoning, to mean lithospheric thermal gradients of no greater than 5 to 6 K/km and heat flow values less than 20-24 mW/m^2 (Solomon and Head, 1989). For the Tharsis Montes and Alba Patera the mechanical lithosphere thickness is likely governed by the strength of crustal material. The mean thermal gradients consistent with the values of T_e for these loads under this assumption fall in the range 10 to 20 K/km and heat flow values in the range 25-50 mW/m^2 (Solomon and Head, 1989). Essentially contemporaneous temperature differences of at least 400 K at 30-40 km depth are implied at a late stage in the development of the Tharsis province. Such temperature differences are too large to be solely the effect of large impacts that occurred some 10^9 yr earlier (Bratt et al., 1985), but they are broadly similar to the temperature variations associated with lithospheric reheating beneath hot spot volcanic centers on Earth (McNutt, 1987). The temperature and heat flow anomalies beneath the central regions of major volcanic provinces on Mars are presumably also related to mantle

dynamic processes, such as convective upwelling plumes and magmatism. Lithospheric thinning beneath the central regions of major volcanic provinces by hot upwelling mantle plumes can account for the different estimates of elastic lithosphere thickness in these regions as compared with the global average.

Mantle Heat Sources

Of particular importance to the thermal evolution of Mars are the concentrations of the radiogenic heat-producing elements K, Th and U in the Martian mantle. Estimates of the abundances of these elements have been made by Taylor (1986), Treiman et al. (1986), and Laul et al. (1986) using SNC meteorites. Taylor (1986) plots analyses of the meteorites on a K/U versus K diagram and shows that the SNC meteorite data are consistent with Earth data. The K/U ratio in Mars is not distinguishable from the Earth's, but this analysis does not yield information on the bulk K abundance in Mars.

Treiman et al. (1986) and Laul et al. (1986) have estimated abundances of K, Th and U using their correlation with other refractory lithophile elements. The data base used by the two sets of authors is substantially the same. Correlations of K with La show that the mantle of Mars has a K/La ratio of about 0.3 of the CI ratio. The corresponding Th/La and U/La ratios are about 1.7 and 2 times the CI ratio, respectively (Treiman et al., 1986). Uncertainties in each estimate are factors of 2, 1.7, and 2, respectively. If the Martian mantle has CI abundances of La, then corresponding abundances of K, Th, and U are about 170 ppm, 48 ppb, and 16 ppb, respectively. If the Martian mantle has higher abundances of La, the abundance of K, Th, and U must be scaled upward accordingly. The bulk Martian abundances must

be reduced in proportion to the mass of the core, assuming that these elements are excluded from the core. The ratios of K/U and Th/U are about 10^4 and 3, respectively, the former being indistinguishable from the Earth's ratio while the latter is lower than the terrestrial value of about four. There is uncertainty in each ratio of about a factor of two based on the scatter in the raw data and an unknown uncertainty in absolute abundances deriving from lack of knowledge of the absolute values of refractory element abundances such as La in Mars relative to CI chondrites.

Laul et al. (1986) derive very similar abundances for the mantle plus crust of Mars for Th and U, but differ by a factor of about two in K. They report K = 315 ppm, Th = 56 ppb, and U = 16 ppb. The K abundance yields a K/U ratio of 2×10^4.

Table 2 summarizes the abundances of radiogenic elements in the Martian mantle estimated from SNC meteorite data. Given the uncertainties in these values, we conclude that radiogenic element abundances in the mantles of Mars and Earth are broadly similar.

THERMAL HISTORY MODELS

On the basis of the constraints discussed in the previous section, we present quantitative simulations of Martian thermal history. In its initial state, Mars is hot and completely differentiated into a core and mantle. The mantle temperature is essentially at the solidus and the core is superliquidus. Radiogenic heat sources are assumed to be distributed uniformly through the mantle, although upward concentration of radioactive elements could accompany differentiation of an early crust. The subsequent evolution consists of a simple cooling, with

monotonic decreases in temperature, heat flux and convective vigor and a monotonic increase in the viscosity of the mantle. We parameterize convective heat transport through the mantle by a simple Nusselt number-Rayleigh number relationship. The parameterization approach is well established as a way of investigating the thermal evolution of the planets (e.g., Schubert et al., 1979; Sharpe and Peltier, 1979; Stevenson and Turner, 1979; Cook and Turcotte, 1981). We employ two different parameterization schemes. With the parameterization model of Stevenson et al. (1983) we focus on the cooling of the core, the extent of core solidification, and the generation of a planetary magnetic field by a core dynamo. With the parameterization model of Turcotte et al. (1979) we emphasize crustal differentiation.

Coupled Core-Mantle Evolution

The planetary thermal history model of Stevenson et al. (1983) is employed in this section to study the consequences of core cooling for the thermal and physical state of the Martian core and the generation of a magnetic field by thermal or chemical compositional convection in the core. The model includes: (1) mantle radiogenic heat production, (2) a mantle viscosity directly proportional to exp(H/RT), where H is a constant activation enthalpy, T is mantle temperature, and R is the gas constant, (3) heat transfer by whole-mantle subsolidus convection parameterized by a Nusselt number-Rayleigh number relation, (4) coupled energy balance equations for the mantle and core, (5) possible inner core freezeout with exclusion of a light-alloying element (most likely sulfur) which then mixes uniformly through the outer core, and (6) realistic pressure- and composition-dependent freezing curves for the core. More detailed information about the model equations and

parameter values can be found in Stevenson et al. (1983) and Schubert and Spohn (1990), who have recently extended the Mars model to include lithospheric growth and the magnetic dipole moment. The solutions we discuss below are actually new calculations, based on the Mars model of Schubert and Spohn (1990), of cases that are almost identical to ones presented in Stevenson et al. (1983). Parameter values are given in Stevenson et al. (1983) and Schubert and Spohn (1990).

Model cooling histories of Mars are typified by the results in Figure 3, which shows mantle heat flow versus time for models with initial core sulfur concentrations x_s of 10 and 25 weight percent (sulfur is assumed to be the light-alloying element in the core in these models). The models with x_s = 10% and 25% are essentially identical to models M1 and M2, respectively, of Stevenson et al. (1983). During the first few hundred million years of evolution, when the planet is hot and its mantle is convecting particularly vigorously, there is a dramatic decrease in heat flow. Following this early period of rapid cooling is a phase of gradual, slow cooling lasting most of the geological life of the planet. The present heat flow in these models is about 30 mW m^{-2}.

The decrease of mantle temperature with time in these models (Figure 4) occurs, like the mantle heat flow, in an early period of short and dramatic temperature reduction followed by a decrease of only 200 to 300 K over the last 4 Gyr of the planet's history. The lithospheres in these models grow to thicknesses of about 100 km at the present (Figure 5). Lithosphere thickness and mantle heat flow and temperature are largely independent of the sulfur concentration in the core. The models have thermal boundary layers at the base of the mantle

that at present are about 100 km thick. Relatively small temperature increases across these bottom boundary layers raise the present core-mantle boundary temperatures of the models about 100 K above the mantle temperatures.

The present lithosphere thicknesses in the models of Figure 5 are smaller, by perhaps a factor of two or more, than what would be expected based on our discussion of lithospheric thickness in the previous section. The lithophere thickness calculated in the models is the thickness of the rheological lithosphere. It is assumed in the models of Figure 5 that a temperature of 1073 K marks the base of the rheological lithosphere. At temperatures larger than 1073 K the Martian mantle is taken to be readily deformable on a geologic time scale. Lithosphere thickness is strongly dependent on the concentration of radiogenic heat sources in the mantle. If the mantle heat source density were half the value assumed in the models of Figure 5, consistent with the estimates of mantle heat source densities from SNC meteorite data (refer to our discussion in the previous section), then the present lithsphere thickness would be about 200 km (Spohn, 1990). Lithosphere thickness would also be increased by magmatic heat transfer (Spohn, 1990) and by upward differentiation of radiogenic heat sources from the mantle into the crust. Thermal history models discussed later in this paper demonstrate that depletion of mantle heat sources with time as a consequence of crustal differentiation results in a thicker lithosphere at present. The present lithosphere thicknesses calculated in the models of Schubert et al. (1979) are representative of maximum thicknesses since those models contained no mantle heat sources.

The decrease with time in the heat flow from the core is shown in

Figure 6 for models with x_s = 10% and 25%. Inner core growth in the x_s = 10% model is marked by the sudden change in the rate of core cooling at about 1.3 Gyr after core cooling begins. After 4.5 Gyr, the inner core in this model is about 920 km in radius, leaving an outer liquid core about 670 km thick. When inner core growth in this model begins, the core heat flow is above the estimated value of heat flow conducted along the core adiabat (the upper dashed curve in Figure 6). Convection in the outer core after about 1.3 Gyr is maintained by both thermal and chemical buoyancy, the latter arising from the release of gravitational potential energy upon concentration of the light-alloying element into the outer core. The slow decline in core heat flow after about 1.3 Gyr is mainly a consequence of latent heat and gravitational energy release upon inner core growth. Core heat flow in the x_s = 10% model falls below the heat flow conducted along the adiabat just after 4.5 Gyr. Core convection beyond 4.5 Gyr would still occur but it would be driven entirely by compositional buoyancy. Thermal convective transport after 4.5 Gyr would actually be downward in the core, but the compositional buoyancy would be adequate to offset th slightly stable thermal state. In the x_s = 10% model, a magnetic field would be generated by thermal convection prior to inner core solidification at about 1.3 Gyr. Both thermal and chemical convection would support a dynamo for times between 1.3 and 4.5 Gyr. Subsequent to 4.5 Gyr a magnetic field would be produced by compositionally driven convection associated with inner core growth.

The sulfur-rich model (x_S = 25%) does not nucleate an inner core. Thermal convection ceases in this model after about 2.7 Gyr, when the core heat flux falls below the heat flux conducted along the core adiabat (lower dashed curve in Figure 6). There is no dynamo action in the core

or planetary magnetic field subsequent to 2.7 Gyr. Stevenson et al. (1983) have used the results of the model calculation with x_s = 25% to estimate the smallest initial sulfur fraction for which no inner core freezeout would occur after 4.5 Gyr; they obtain a value of about 15 weight percent S.

Schubert and Spohn (1990) have carried out a number of additional Martian thermal history calculations with a view toward more carefully delineating conditions for no inner-core freezeout. Their results are shown in Figure 7, which gives the dependence of present inner-core radius (as a fraction of total core radius) on both present mantle viscosity and initial weight percent sulfur x_s in the core. Present inner-core radius increases with decreasing x_s for a given present mantle viscosity since decreasing x_s increases the core melting temperature and results in earlier inner-core freezeout and a longer time for inner-core growth. Present inner-core radius also increases with decreasing present mantle viscosity at fixed x_s since cooling is more rapid with lower mantle viscosity resulting in earlier inner-core freezeout and a longer period of inner-core growth. Fifteen weight percent is a good estimate of the minimum core sulfur concentration required for no core freezing through geologic time. However, core freezing would occur for x_S larger than 15 weight percent if the present mantle viscosity is less than about $10^{16} m^2 s^{-1}$ (or about 3.5 x 10^{19} Pa s for a mantle density of 3500 kg m^{-3}).

Figure 8, after Schubert and Spohn (1990), shows inner core radius versus time for three different initial S concentrations. Inner core growth is very rapid once freezeout begins; the inner core is almost completely grown within 0.5 to 1 Gyr of initial freezeout. The

depression of the melting temperature in the outer core as the sulfur concentrates there with progressive inner core growth and the slowing of the cooling rate as the planet evolves both contribute to the reduction in inner core growth rate with time. With increasing x_S, the time of initial core freezeout is delayed and present inner core radius decreases.

If the estimates of Laul et al. (1986) and Treiman et al. (1987) of 14 and 12.5 weight percent S in the Martian core are taken to imply that x_S is less than about 15 weight percent, then based on Figure 7, it is likely that Mars has a solid inner core. If Mars has no magnetic field, the explanation may then lie in the nearly complete solidification of the core (Young and Schubert, 1974). On the other hand, if the Laul et al. (1986) and Treiman et al. (1987) predictions of weight percent S in the Martian core are underestimates, then according to Figure 7, Mars would not have a solid inner core at present, and the explanation for lack of a present Martian magnetic field might lie in the absence of a drive (a growing inner core) for chemical convection in a core that had cooled too far to thermally convect at present (Stevenson et al., 1983). Our knowledge of Mars is inadequate to unambiguously distinguish between these alternative possibilities, although complete freezing of the Martian core probably requires an unreasonably low content of S in the core. The thermal history models are also consistent, depending on the real value of x_S in the Martian core, with a Mars that presently has a growing solid inner core, a dynamo in its liquid outer core driven by chemical compositional convection, and a planetary magnetic field, albeit a small one. Figure 7 shows that if x_S is less than about 15 weight

percent, but not too small, then the core of Mars would only be partially solidified at present and a Martian dynamo and magnetic field would be likely.

This is illustrated in Figure 9, which shows the results of a model calculation of the Martian magnetic dipole moment μ_M, normalized with respect to the Earth's present magnetic dipole moment, as a function of time for the Mars models with x_s = 10% and 25%. The calculation of μ_M follows Stevenson et al. (1983) and Schubert and Spohn (1990). The magnetic dipole moment decreases rapidly during the first several hundred million years of evolution following the early rapid cooling of the planet and the rapid decline in core heat flow. With x_S = 10%, dynamo action occurs throughout the planet's evolution. Prior to 1.3 Gyr, the model Martian dynamo is driven by thermal convection in the core. There is a sudden increase in μ_M at about 1.25 Gyr coincident with inner core formation. Subsequent to 1.3 Gyr, the dynamo is driven by both thermal and chemical compositional convection as the inner core solidifies and releases latent heat and gravitational potential energy. With x_S = 25% there is no inner core solidification and the dynamo is driven solely by thermal convection until about t = 2.7 Gyr when dynamo action ceases because the core heat flux falls below the conductive heat flux along the core adiabat and thermal convection can no longer occur in the core. There is no present magnetic field in this model of Martian evolution because thermal convection is not possible in the present liquid core and there is no source of chemical convection in the core. Because of the uncertainty in the exact value of the conductive heat flux along the Martian core adiabat (Schubert and Spohn, 1990), we cannot exclude the possibility that at present there

is a weakly thermally convecting liquid core in Mars and a weak dynamo. If it should be determined that Mars has a small magnetic field, then such a model would provide a plausible explanation.

Crustal Differentiation

Magmatism in planetary interiors results in crustal formation and the removal of heat-producing radiogenic elements from the planetary mantle. The removal of heat sources reduces the vigor of mantle convection, allows the mantle to cool more rapidly, increases the lithosphere thickness, and reduces surface volcanism. In this section we provide quantitative estimates of the rate of crustal magmatism by extending the approach of Turcotte et al. (1979) to the parameterization of convective cooling in the mantle of Mars. We refer the reader to Turcotte and Huang (1990) for the details of this approach and discuss here only the modifications necessary to simulate crustal production and the depletion of the mantle in radiogenic heat sources. A recent study of Martian thermal history with crustal differentation has also been carried out by Spohn (1990).

In order to model the loss of heat-producing elements from the interior of Mars to its crust by magma transport, we take the rate of internal heat generation per unit mass H to be given by

$$\frac{dH}{dt} = -H\{\lambda + \frac{\chi u}{R}\} \qquad (3)$$

where t is time, λ is the radioactive decay rate ($2.77 \times 10^{-10} yr^{-1}$, Turcotte and Schubert, 1982), u is a mean convective velocity in the mantle, R is the radius of Mars, and χ is a crustal fractionation parameter. The parameter χ is the ratio of the characteristic turnover time for mantle convection to the characteristic time for crustal

fractionation. Based on the present rate of formation of the oceanic crust on the Earth, we show below that $\chi = 0.01$ for the Earth. Of course, the crustal fractionation model developed here is not applicable to the Earth because crustal recycling through subduction is occurring.

If the crustal fractionation parameter is sufficiently large then the planet will be fully differentiated. If f is the fraction of crustal material available, then the maximum thickness of crust D_{co} that can be formed is

$$D_{co} = \frac{f\rho_m R}{3\rho_c} \quad . \tag{4}$$

In deriving (4) we have neglected the volume of the core. With f = 0.1, mantle density $\rho_m = 3940$ kg m^{-3}, crustal density $\rho_c = 2900$ kg m^{-3}, and R = 3398 km, we find that $D_{co} = 154$ km. The thickness of the evolving crust is assumed to be given by

$$D_c = D_{co}\left(1 - \frac{H}{H_e}\right) \quad , \tag{5}$$

where H_e is the rate of heat generation in the interior without any crustal extraction given by

$$H_e = H_o\, e^{-\lambda t} \tag{6}$$

and $H_o = 2.47 \times 10^{-11}$ W kg^{-1} (based on estimates for the Earth; Turcotte and Schubert, 1982).

Removal of radioactive elements from the mantle through crustal differentiation affects the growth of the lithosphere by reducing the heat flux from the mantle that must be conducted across the lithosphere. We assume that the heat-producing elements in the crust are sufficiently near the surface that they do not influence the

conductive gradient; the base of the lithosphere is defined to lie at a temperature T_r. With these assumptions, the thickness of the conductive lithosphere is given by

$$D_L = \frac{T_r - T_s}{\frac{R}{3}\left(\frac{\rho_m H}{k} - \frac{1}{\kappa}\frac{dT}{dt}\right)} \quad , \tag{7}$$

where k is the thermal conductivity, κ is the thermal diffusivity, and T_s is the surface temperature. The denominator is related to the heat flow through the lithosphere.

The volumetric rate $\dot{V}_v$ of addition of magma to the crust can be determined through its relation to the change in crustal thickness by

$$\dot{V}_v = 4\pi R^2 \frac{dD_c}{dt} \quad . \tag{8}$$

The parameterized convection calculations can also be used to determine whether the radius of the planetary body is increasing or decreasing. The appropriate relation is

$$\frac{\delta R}{R} = -\frac{\alpha}{3}\left[T_o - T\left(1 - \frac{3}{2}\frac{D_L}{R}\right)\right] + \frac{\Delta\rho D_c}{3D_{co}} \tag{9}$$

where T_o is the initial temperature of the planet, α is the volumetric coefficient of thermal expansion, and $\Delta\rho$ is the decrease in density associated with crustal differentiation. The first term on the right of (9) follows from (2) and the second term represents the increase in volume associated with crustal formation.

We present results of planetary evolution calculations for the following parameter values: $\kappa = 10^{-6}$ m^2 s^{-1}, thermal conductivity k = 4 W m^{-1} K^{-1}, T_r = 1000 K, T_s = 255 K, T_o = 2,000 K, $\alpha = 3 \times 10^{-5}$ K^{-1}, and $\Delta\rho$ = 80 kg m^{-3}. The mean mantle temperature, crustal thickness, rate of volcanism, litho- sphere thickness, surface heat flow, and fractional

radius change are given in Figures 10 to 15 as functions of time for various values of the crustal fractionation parameter χ in the range 0 to 10^{-2}.

The extraction of heat-producing elements into the crust can have important effects on the thermal evolution of Mars. Most of the crustal growth occurs early in the evolution of Mars, i.e., within several hundred million years of the end of accretion (Figure 11). This is in accord with the evidence discussed earlier of an age $\geq$ 4 Gyr for the southern crustal highlands. The present mean crustal thickness depends on the choice of the crustal fractionation parameter χ.

We can estimate the value of the crustal fractionation parameter for the Earth, since it is the ratio of crustal fractionation time $V_e/\dot{V}_c$ to characteristic mantle turnover time R/u ($\dot{V}_c$ is the volumetric fractionation rate of the mantle and V_e is the volume of the mantle). Taking the rate of formation of oceanic crust to be 2.8 km^2/yr and the depth processed to be 60 km, we have $\dot{V}_c$ = 168 km^3/yr. With V_e = $10^{12} km^3$, we find that the characteristic time for creation of the oceanic crust is $V_e/\dot{V}_c$ = 6 Gyr. With R = 5,800 km (approximately twice the mantle thickness) and u = 0.1 m/yr we find that the characteristic mantle turnover time is R/u = 58 Myr. Thus we find that χ is about 0.01 for the Earth at the present time.

The crustal thickness on Mars has been estimated using gravity data and Airy isostasy. For Hellas Planitia, Sjogren and Wimberly (1981) found that the depth of compensation is 130 km. For the crater Antoniadi, Sjogren and Ritke (1982) found that the depth of compensation is 115 km. From gravity profiles across the highland-lowland escarpment, Janle (1983) found that the depth of compensation

is also 115 km. Taking the crustal thickness to be D_c = 120 km, we find from Figure 11 that the corresponding crustal fractionation factor is χ = 0.003, about a factor of three less than we found for the Earth. This estimate of χ is uncertain because of the poorly constrained value of the mean crustal thickness on Mars.

Accepting, for purposes of discussion, that the crustal fractionation factor for Mars is χ = 0.003, we can determine rates of crustal addition from Figures 11 and 12. The average amount of crust added in the last billion years (0 - 1 Gyr BP) was 600 m, the average amount of crust added between 1 - 2 Gyr BP was 1.8 km, and the average amount of crust added between 2 - 3 Gyr BP was 2.9 km. The volumetric rate of crustal magmatism was much higher early in the evolution of Mars. The decline to the lower values of crustal production rate characteristic of most of Mars geologic history occurred with about a 100 Myr time scale.

A detailed summary of the stratigraphy of Mars has been given by Tanaka (1986). Relative ages are quite tightly constrained by crater counts, but absolute ages are uncertain due to uncertainties in the volcanic flux. The most recent volcanism is associated with the Upper Amazonian period. Volcanics of this period are associated with the Arcadia, Olympus Mons, Medusae Fossae, and Tharsis Montes Formations, but the principal volcanics are flood basalts in the southern Elysium Planitia. These have an area of 100,000 km^2, but Tanaka (1986) suggests that the thickness is only a few tens of meters. Taking a thickness of 50 m, this is only 0.03 m when averaged over the surface of Mars.

Greeley (1987) has estimated that 26 x 10^6 km^3 of volcanics erupted

during the Middle and Upper Amazonian. This corresponds to a mean thickness of 200 m when averaged over the entire surface of Mars. Based on the meteorite flux intensity given by Hartmann et al. (1981), the Upper Amazonian extends from 0 to 0.7 Gyr BP and the Middle Amazonian from 0.7 to 2.3 Gyr BP. Thus, the young volcanics on Mars are consistent with our results since volcanism represents only a part of crustal addition. It should be emphasized, however, that there are considerable uncertainties in the absolute ages and in the crustal fractionation parameter.

Other predictions of our calculations using $\chi = 0.003$ are a lithospheric thickness $D_L = 400$ km and a net global contraction corresponding to $\delta R/R = -0.001$. From Figure 15 we see that a global expansion of $\delta R = 10$ km occurred in the first 200 Myr of the evolution of Mars. This expansion was caused by the density change associated with the generation of the early crust. For the remainder of the evolution of Mars, a nearly steady contraction occurred associated with the cooling of the interior. The total contraction subsequent to the period of early crustal differentiation was $\delta R = -13$ km. All models in Figure 15 with substantial crustal fractionation show an early period of planetary expansion followed by a larger amount of planetary contraction.

The surface tectonic features of Mars include both extensional features and compressional features. Much of the evidence for lithospheric extension on Mars is provided by graben systems in and near the Tharsis region. These features are likely to be the result of the stresses generated by the Tharsis load. Wrinkle ridges occur commonly throughout ancient terrains. These can be attributed to the

thermal contraction illustrated in Figure 15.

Models of the response of Mars to the long wavelength topographic load of the Tharsis rise provide a reasonable fit to the observed gravity if the elastic lithosphere of Mars was globally in the range 100 to 400 km when the Tharsis construct formed (Banerdt et al., 1982; Willemann and Turcotte, 1982). Since the elastic lithosphere is generally about one half the thickness of the thermal lithosphere, these values are consistent with those given in Figure 13. All models in Figure 13 with large lithosphere thicknesses show substantial depletion in mantle radioactivity due to crustal differentiation. For no crustal differentiation, the lithosphere thickness from Figure 13 is about 100 km, in agreement with the result previously obtained in Figure 5.

It is widely accepted that the crust of Mars has a generally basaltic composition consistent with the fractionation of the mantle associated with mantle convection. The amounts of more recent volcanism on Mars are also consistent with our model.

PATTERNS OF MANTLE CONVECTION

Numerical calculations of fully three-dimensional convection in a spherical shell were recently carried out by Schubert et al. (1990) to simulate possible convective planforms in the Martian mantle. These results have important implications for proposed convective origins for major geologic features on Mars, such as the crustal dichotomy. The reader is referred to Schubert et al. (1990) for more detailed information about the calculations than can be provided here.

The spherical shell model of the Martian mantle consists of a Boussinesq fluid that is heated both internally and from below to

account for secular cooling, radiogenic heating and heat flow from the core. The lower boundary of the shell is assumed to be isothermal and stress-free, as appropriate to the interface between the mantle and a liquid outer core. The upper boundary of the shell is rigid and isothermal, as appropriate to the base of a thick, immobile lithosphere. The ratio of the inner radius of the shell to its outer radius is 0.55, in accordance with possible core radii in Mars. We present results for two different modes of heating. In one case, 20 percent of the surface heat flow originates in the core, and in the other case the percentage of heating from below is 94 percent. The Rayleigh numbers of both cases are approximately one hundred times the critical Rayleigh numbers that characterize the onset of convection in the constant-viscosity spherical shells. These Rayleigh numbers may be an order of magnitude or more smaller than the Rayleigh number of the Martian mantle. However, the Rayleigh number of the Martian mantle is unknown because of uncertainties in the thickness of the mantle and its material properties, viscosity in particular. The numerical approach is described in detail in Glatzmaier (1988) and Bercovici et al. (1989a). Table 3 lists the parameter values for the calculations discussed here.

The horizontal planforms of convection for both modes of heating are illustrated in Figure 16 by contours of radial velocity on spherical surfaces midway through the shells. Meridional cross-sections of entropy contours (equivalent to isotherms in these Boussinesq calculations) for both heating modes are shown in Figure 17. The prominent form of upwelling in the Martian mantle is the cylindrical plume. The number of upwelling plumes is strongly

influenced by the mode of heating; with only 20 percent heating from below there are a dozen plumes, while 94 percent bottom heating produces only six plumes. There are fewer, stronger plumes as the proportion of bottom heating increases. Plumes carry the heat flow from the core and arise from instability of the lower thermal boundary layer at the core-mantle interface. In general, the fraction of mantle heating delivered from the core has probably decreased with time as the core cooled to temperatures not much greater than those of the lower mantle (e.g., Figure 6). The isotherm cross-sections of Figure 17 show several plumes originating in the lower thermal boundary layer. Convective downwelling occurs in planar sheets that form an interconnected network surrounding the upwelling plumes. The downwellings also show cylindrical concentrations along the sheets and even distinct cylindrical downwellings.

The patterns of Figure 16 have evolved through many overturns of the mantle and the solutions appear to be fundamentally time dependent. However, the basic nature of the convective planform, i.e., cylindrical upwelling plumes surrounded by planar downwelling sheets, does not change with time. Thus, we can expect major volcanic provinces on Mars, like Tharsis and Elysium, to reflect the cylindrical nature of upwelling mantle plumes, similar to hotspots on Earth. There are no sheetlike upwelling features in the Martian mantle to produce a pattern similar to the linear global system of mid-ocean ridges on the Earth. Even the mid-ocean ridges on Earth are not connected to deep sheetlike upwellings in the Earth's mantle (Bercovici et al., 1989b). The deep upwellings in models of convection in the Earth's mantle are also cylindrical plumes. The Earth's mid-ocean ridges are shallow, passive

upwellings occurring in response to the tearing of lithospheric plates by the pull of descending slabs (Bercovici et al., 1989b). The non-Newtonian rheology of the Earth's lithosphere is essential for the occurrence of plate tectonics. Mars is a one-plate planet with a thick lithosphere (Solomon, 1978; Schubert et al., 1979) beneath which mantle upwellings are in the form of cylindrical plumes.

The results of the spherical convection models have implications for proposed explanations of the crustal dichotomy and the concentrations of volcanism at Tharsis and Elysium. If the crustal dichotomy was caused by a convective system dominated by spherical harmonic degree $\ell = 1$ (Schubert and Lingenfelter, 1973; Lingenfelter and Schubert, 1973; Wise et al., 1979b) with upwelling under the northern hemisphere, then the convection must have been driven strongly from below (while our models produced six to twelve plumes, the number of plumes decreases with increasing percentage of bottom heating). Such strong heating concentrated deep within Mars can arise from the heating pulse accompanying core formation or from the flow of heat from a hot core. Indeed, the overturning accompanying core formation could in itself be an $\ell = 1$ mode (Stevenson, 1980), obviating the need for a thermally driven motion.

Core size is another important factor in determining the number of convective plumes. With smaller cores there is a tendency toward fewer upwelling plumes (Zebib et al., 1983). This is confirmed by the results of Figure 18, which shows mid-depth radial velocity contours and isotherms in meridional cross-section in the mantle of a Mars model with a core radius 0.2 times the radius of Mars (Schubert et al., 1990). The model has settled into a predominantly $\ell=2$ (not $\ell=1$,

however) convection pattern. During the early stages of core formation, the effective core radius would have been smaller than the radius at present, favoring a thermally forced convection with perhaps just one dominant upwelling. Since the Martian core formed contemporaneously with accretion or within a few hundred million years of the end of accretion, conditions favoring ℓ=1 convection, i.e., a small core and a deep heat source, occur very early in the evolution of Mars. If a convective mechanism is responsible for the crustal dichotomy, then the dichotomy must also be a very ancient feature.

It is not obvious from the models why there should be only two major volcanic centers (Tharsis and Elysium) on Mars. The models predict several to about ten major mantle plumes. Perhaps the models are not realistic enough to predict the actual number of major hotspots on Mars. On the other hand, there may be many plumes in the Martian mantle, but the properties of the lithosphere may select only one or two of them for prominent surface expression. Plume activity could be focussed beneath Tharsis if fracturing or thinning of the lithosphere in this region has facilitated magma and heat transport across the lithosphere. The temperature dependence of mantle viscosity will strongly influence the structure of plumes and their number, through the control that variable viscosity exerts on the nature and vigor of small scale convective activity in the lower thermal boundary layer (Olson et al., 1987).

The numerical solutions discussed above can be used to infer that several kilometers of dynamic topography could be associated with plumes in the Martian mantle (Schubert et al., 1990). Dynamic uplift is insufficient to account for the 10 km of topography in the Tharsis

region. This large topographic excess must be largely the result of other processes, such as volcanic construction, magmatic thickening of the crust, or depletion of the underlying mantle (e.g., Sleep and Phillips, 1979, 1985; Solomon and Head, 1982). Nevertheless, it is likely that the Tharsis rise and its volcanic constructs are a consequence of a strong mantle plume (or grouping of plumes) beneath the region.

Conclusions

Several themes emerge from this overview of the thermal history of Mars. The first is the hot initial state of the planetary interior and the sharp contrasts that can be drawn between the first 1 Gyr of Martian history and the subsequent 3.5 Gyr. As a result of accretional heating and core formation essentially contemporaneous with planetary formation, the early history of Mars was characterized by high internal temperatures, a vigorously convecting mantle, and high surface fluxes of heat and magma. Outgassing contributed to an early atmosphere, and widespread magmatism may have helped trigger the release of subsurface water and large-scale floods. Parameterized convection models indicate, however, that on a time scale of only a few hundred million years the mantle convective engine slowed, as primordial interior heat was lost and as radioactive heat production decayed or was concentrated into the shallow crust. Rapid interior cooling led to a globally thick lithosphere and was accompanied by global contraction, recorded in the pervasive formation of wrinkle ridges now preserved on ancient geological units. The last 3.5 Gyr of Martian history was marked, in contrast, by slow cooling and by the concentration of volcanic and

tectonic activity in ever more limited regions.

The second theme of Martian thermal history is the strong role of lumes expected for mantle convection. As long as a significant fraction of mantle heating comes from the core, three-dimensional convection calculations indicate that plumes dominate the upwelling portions of the flow. At least some of those plumes would be expected to have strong signatures in the surface topography and volcanic flux. The Tharsis and Elysium volcanic provinces are probably the consequences of plume-delivered heat and magma. The number and characteristics of plumes depend on the relative contributions of radioactivity and core cooling to the mantle heat budget, as well as the size of the core. While current models do not predict as few as two dominant plumes or plume families, development of Tharsis and Elysium very early in Martian history, when core cooling occurred at its highest rate, is favored.

A third theme of this overview is the dominating influence of core sulfur concentration on the thermal evolution of the core and the history of the Martian magnetic field. A core with more than about 15 weight percent S probably would not crystallize a solid inner core and probably would not be thermally convecting at present. This critical S concentration is tantalizingly close to estimates of the core sulfur content from elemental abundances of SNC meteorites. Therefore, a nearly completely fluid core that is nonconvecting or only weakly thermally or chemically convecting may provide an explanation for the lack of a present Martian magnetic field or the existence of a very weak one.

A final theme of this overview is the strong impact that new

information from Mars would have on our understanding of the origin and thermal evolution of the planet. Detection of an internal magnetic field or evidence for a paleofield would strongly constrain the evolution of the Martian core. Seismic determination of the thickness of the crust would provide a crucial tie point to discussions of the planetary magmatic budget, and a seismic estimate of the radius and state of the core would enable a considerably more confident assessment of bulk composition. Measurement of surface heat flow would substantially constrain the present mantle heat production. Finally, the return of Martian igneous rocks to terrestrial laboratories would provide crucial knowledge of the detailed absolute time scale for the major events in the history of the planet.

Acknowledgments

We thank Tilman Spohn for recalculating the models of Figures 3-6, partial results of which were originally presented in Stevenson et al. (1983). This work was supported by NASA through grants NSG 7315 (G. S.), NAG 9-39 (M. J. D.), and NAG 5-814 and NSG 7297 (S.C.S.).

References

Anderson, D. L., Miller, W. F., Latham, G. V., Nakamura, Y., Toksöz, M. N., Dainty, A. M., Duennebier, F. K., Lazarewicz, A. R., Kovach, R. L. and Knight, T. C. D. 1977. Seismology on Mars. *J. Geophys. Res.* 82: 4524-4546.

Arvidson, R. E., Goettel, K. A. and Hohenberg, C. M. 1980. A post-Viking view of Martian geologic evolution. *Rev. Geophys. Space Phys.* 18: 565-603.

Banerdt, W. B., Phillips, R. J., Sleep, N. H. and Saunders, R. S. 1982. Thick-shell tectonics on one-plate planets: Applications to Mars. *J. Geophys. Res.* 87:9723-9733.

Basaltic Volcanism Study Project. 1981. *Basaltic Volcanism on the Terrestrial Planets*, Pergamon, New York, 1286 pp.

Becker, R. H. and Pepin, R. O. 1984. The case for a Martian origin of the shergottites: Nitrogen and noble gases in EETA 79001, *Earth Planet. Sci. Lett.* 69:225-242.

Bercovici, D., Schubert, G., Glatzmaier, G. A., and Zebib, A., 1989a. Three-dimensional thermal convection in a spherical shell. *J. Fluid Mech.*, 206:75-104.

Bercovici, D., Schubert, G., and Glatzmaier, G. A., 1989b. Three-dimensional spherical models of convection in the Earth's mantle. *Science* 244:950-955.

Bills, B. G. 1989. The moments of inertia of Mars. *Geophys. Res. Lett.*, 16:385-388.

Bills, B. G. and Ferrari, A. J. 1978. Mars topography harmonics and geophysical implications. *J. Geophys. Res.* 83: 3497-3508.

Binder, A. B. and Davis, D. R. 1973. Internal structure of Mars. *Phys. Earth Planet. Inter.* 7:477-485.

Blasius, K. R. and Cutts, J. A. 1976. Shield volcanism and lithospheric structure beneath the Tharsis plateau, Mars. *Proc. Lunar Sci. Conf.* 7:3561-3573.

Bogard, D. D., Nyquist, L. E. and Johnson, P. 1984. Noble gas contents of shergottites and implications for the Martian origin of SNC meteorites. *Geochim. Cosmochim. Acta* 48: 1723-1740.

Bratt, S. R., Solomon, S. C. and Head. J. W. 1985. The evolution of

impact basins: Cooling, subsidence, and thermal stress. *J. Geophys. Res.* 90:12415-12433.

Carr, M. H. 1973. Volcanism on Mars. *J. Geophys. Res.* 78:4049-4062.

Carr, M. H. 1974. Tectonism and volcanism of the Tharsis region of Mars. *J. Geophys. Res.* 79:3943-3949.

Carr, M. H. 1976. Change in height of Martian volcanoes with time. *Geol. Rom.* 15:421-422.

Carr, M. H. 1987. Water on Mars. *Nature* 326:30-35.

Carr, M. H., Greeley, R., Blasius, R., Guest, J. E. and Murray, J. B. 1977. Some Martian volcanic features as viewed from the Viking orbiters. *J. Geophys. Res.* 82:3985-4015.

Carr, M. H., Masursky, H. and Saunders, R. S. 1973. A generalized geologic map of Mars. *J. Geophys. Res.* 78:4031-4036.

Chapman, C. R. 1974. Cratering on Mars, I and II. *Icarus* 22:272-291.

Chen, J. H. and Wasserburg, G. J. 1986. Formation ages and evolution of Shergotty and its parent from U-Th-Pb systematics, *Geochim. Cosmochim. Acta* 50:955-968.

Chicarro, A. F., Schultz, P. H. and Masson, P. 1985. Global and regional ridge patterns on Mars. *Icarus* 63: 153-174.

Cisowski, S. M. 1981. Magnetic properties of Shergotty and Zagami meteorites. *Lunar Planet Sci.* XII:147 (abstract).

Cisowski, S. M. 1982. Magnetic properties and remanence of Antarctic shergottite A79001. *Lunar Planet Sci.* XIII:106 (abstract).

Comer, R. P., Solomon, S. C. and Head, J. W. 1985. Mars: Thickness of the lithosphere from the tectonic response to volcanic loads, *Rev. Geophys.*, 23:61-92.

Cook, F. A., and Turcotte, D. L. 1981. Parameterized convection and

the thermal history of the Earth. *Tectonophysics* 75:1-17.

Coradini, A., Federico, C. and Lanciano, P. 1983. Earth and Mars: Early thermal profiles. *Phys. Earth Planet. Int.* 31: 145-160.

Crisp, J. 1984. Rates of magma emplacement and volcanic output. *J. Volcanol. Geotherm. Res.* 20:177-211.

Davies, G. F. and Arvidson, R. E. 1981. Martian thermal history, core segregation, and tectonics. *Icarus* 45: 339-346.

Dolginov, Sh. Sh. 1987. What have we learned about the Martian magnetic field? *Earth Moon Planets* 37:17-52.

Dolginov, Sh. Sh., Yeroshenko, Ye. G. and Zhuzgov, L. N. 1973. The magnetic field in the very close neighborhood of Mars according to data from the Mars 2 and Mars 3 spacecraft. *J. Geophys. Res.* 78:4779-4786.

Dolginov, Sh. Sh., Yeroshenko, Ye. G. and Zhuzgov, L. N. 1976. The magnetic field of Mars according to the data from the Mars 3 and Mars 5 spacecraft. *J. Geophys. Res.* 81:3353-3362.

Glatzmaier, G. A. 1988. Numerical simulations of mantle convection: Time-dependent, three-dimensional, compressible, spherical shell. *Geophys. Astrophys. Fluid Dyn.* 43:223-264.

Goettel, K. A. 1981. Density of the mantle of Mars. *Geophys. Res. Lett.* 8: 497-500.

Goins, N. R., and Lazarewicz, A. R. 1979. Martian seismicity. *Geophys. Res. Lett.* 6: 368-370.

Greeley, R. 1987. Release of juvenile water on Mars: Estimated amounts and timing associated with volcanism. *Science* 236:1653-1654.

Harris, A. W. and Ward, W. R. 1982. Dynamical constraints on the formation and evolution of planetary bodies. *Ann. Rev. Earth Planet*

Sciences. 10:61-108.

Hartmann, W. K. 1973*a*. Martian cratering, 4, Mariner 9 initial analysis of cratering chronology. *J. Geophys. Res.* 78:4096-4116.

Hartmann, W. K. 1973*b*. Martian surface and crust: Review and synthesis. *Icarus* 19:550-575.

Hartmann, W. K. 1977. Relative crater production rates on planets. *Icarus* 31:260-276.

Hartmann, W. K., Strom, R. G., Weidenschilling, S. J., Blasius, K. R., Woronow, A., Dence, M. R., Grieve, R. A. F., Diaz, J., Chapman, C. R., Shoemaker, E. M. and Jones, K. L. 1981. Chronology of planetary volcanism by comparative studies of planetary cratering, in *Basaltic Volcanism on the Terrestrial Planets,* Pergamon (New York), 1049-1127.

Hartmann, W. K. and Vail, S. M. 1986. Giant impactors: Plausible sizes and populations. In *Origin of the Moon*, eds. W. K. Hartmann, R. J. Phillips, and G. J. Taylor (Houston: Lunar and Planetary Institute) pp. 551-556.

Janle, P. 1983. Bouguer gravity profiles across the highland-lowland escarpment on Mars. *Moon and Planets* 28:55-67.

Janle, P., and Jannsen, D. 1986. Isostatic gravity and elastic bending models of Olympus Mons, Mars. *Annal. Geophys.* 4B:537-546.

Johnston, D. H., McGetchin, T. R. and Toksöz, M. N. 1974. The thermal state and internal structure of Mars. *J. Geophys. Res.* 79: 3959-3971.

Johnston, D. H., and Toksöz, M. N. 1977. Internal structure and properties of Mars. *Icarus* 32: 73-84.

Jones, J. H. 1986. A discussion of isotopic systematics and mineral zoning in the shergottites: Evidence for a 180 my igneous crystallization age. *Geochim. Cosmochim. Acta* 50:969-977.

Kaula, W. M. 1979*a*. Thermal evolution of Earth and Moon growing by planetesimal impacts. *J. Geophys. Res.* 84:999-1008.

Kaula, W. M. 1979*b*. The moment of inertia of Mars. *Geophys. Res. Lett.* 6:194-196.

Kaula, W. M., Sleep, N. H., and Phillips, R. J. 1989. More about the moment of inertia of Mars. *Geophys. Res. Lett. 16*:1333-1336.

Kobrick, M., Roth, L. E. and Downs, G. S. 1981. A radar redetermination of the Martian center of mass-center of figure offset. *Eos, Trans. Amer. Geophys. Union* 62:942 (abstract).

Laul, J. C., Smith, M.R., Wänke, H., Jagoutz, E., Dreibus, G., Palme H., Spettel B., Burghele, A., Lipschutz, M. E., and Verkouteren, R. M. 1986. Chemical systematics of the Shergotty meteorite and the composition of its parent body (Mars). *Geochim. Cosmochim. Acta* 50: 909-926.

Lingenfelter, R. E., and Schubert, G. 1973. Evidence for convection in planetary interiors from first-order topography. *The Moon* 7:172-180.

Malin, M. C., 1977. Comparison of volcanic features of Elysium (Mars) and Tibesti (Earth). *Geol. Soc. Amer. Bull.* 88:908-919.

McGill, G. E. 1988. The Martian crustal dichotomy. In *Abstracts for the MEVTV-LPI Workshop: Early Tectonic and Volcanic Evolution of Mars.* (Houston: Lunar and Planetary Institute), pp. 42-44 (abstract).

McGovern, P. J., and Schubert, G. 1990. Thermal evolution of the Earth: Effects of volatile exchange between atmosphere and interior. *Earth Planet. Sci. Lett.*, in press.

McNutt, M. 1987. Temperature beneath midplate swells: The inverse problem. In *Seamounts, Islands, and Atolls*, ed. B. H. Keating, P. Fryer, R. Batiza and G. W. Boehlert. *Geophys. Mon.* 43. (Washington,

DC: AGU), pp. 123-132.

McSween, H. Y. Jr. 1984. SNC meteorites: Are they Martian rocks? *Geology* 12:3-6.

Mutch, T. A., and Saunders, R. S. 1976. The geologic development of Mars: A review. *Space Sci. Rev.* 19:3-57.

Neukum, G., and Hiller, K. 1981. Martian ages. *J. Geophys. Res.* 86:3097-3121.

Neukum, G., and Wise, D. U. 1976. Mars: A standard crater curve and possible new time scale. *Science* 194:1381-1387.

Okal, E. A., and Anderson, D. L. 1978. Theoretical models for Mars and their seismic properties. *Icarus* 33: 514-528.

Olson, P., Schubert, G., and Anderson, C. 1987. Plume formation in the D"-layer and the roughness of the core-mantle boundary. *Nature* *327*:409-413.

Ong, M., Luhmann, J. G., Russell, C. T., Schwingenschuh, K., Riedler, W., Yeroshenko, Ye. 1989. Phobos observations of the Martian magnetotail. *Eos, Trans. Amer. Geophys. Union 70*:1174. (abstract)

Owen, T., Maillard, J. P., de Bergh, C. and Lutz, B. L. 1988. Deuterium on Mars: The abundance of HDO and the value of D/H. *Science* 240:1767-1770.

Phillips, R. J., and Saunders, R. S. 1975. The isostatic state of Martian topography. *J. Geophys. Res* 80:2893-2898.

Phillips, R. J., Saunders, R. S. and Conel, J. E. 1973. Mars: Crustal structure inferred from Bouguer gravity anomalies. *J. Geophys. Res.* 78:4815-4820.

Reasenberg, R. D. 1977. The moment of inertia and isostasy of Mars. *J. Geophys. Res.* 82:369-375.

Riedler, W., Schwingenschuh, K., Yeroshenko, Ye., Luhmann, J. G., Ong, M., and Russell, C.T. 1989. The magnetotail of Mars. *Bull Am. Asron. Soc. 21*:1989. (abstract).

Roth, L. E., Kobrick, M., Downs, G. S., Saunders, R. S. and Schubert, G. 1981. Martian center of mass-center of figure offset. In *Reports of Planetary Geology Program - 1981*, NASA TM 84211:372-374 (abstract).

Russell, C. T. 1978. The magnetic field of Mars: Mars 5 evidence re-examined. *Geophys. Res. Lett.* 5:85-88.

Russell, C. T., Luhmann, J. G., Spreiter, J. R., and Stahara, S. S. 1984. The magnetic field of Mars: Implications from gas dynamic modeling. *J. Geophys. Res.* 89:2997-3003.

Schubert, G., Bercovici, D., and Glatzmaier, G. 1990. Mantle dynamics in Mars and Venus: Influence of an immobile lithosphere on three-dimensional convection. *J. Geophys. Res.*, in press.

Schubert, G., Cassen, P., and Young, R. E. 1979. Subsolidus convective cooling histories of terrestrial planets. *Icarus* 38:192-211.

Schubert, G., and Lingenfelter, R. E. 1973. Martian center of mass-center of figure offset. *Nature* 242:251-252.

Schubert, G. and Spohn, T. 1990. Thermal history of Mars and the sulfur content of its core. *J. Geophys. Res.*, in press.

Sharp, R. P. 1973. Mars: Troughed terrain. *J. Geophys. Res.* 78:4063-4072.

Sharpe, H. N. and Peltier, W. R. 1979. A thermal history for the Earth with parameterized convection. *Geophys. J. Roy. Astron. Soc.* 59:171-203.

Shih, C.-Y., Nyquist, L. E., Bogard, D. D., McKay, G. A., Wooden, J.

L., Bansal, B. M., and Weisman, H. 1982. Chronology and petrogenesis of young achondrites, Shergotty, Zagami and ALHA77005: Late magmatism on a geologically active planet. *Geochim. Cosmochim Acta* 46:2323-2344.

Sjogren, W. L. and Ritke, S. J. 1982. Mars: Gravity data analysis of the crater Antoniadi. *Geophys. Res. Let.* 9:739-742.

Sjogren, W. L. and Wimberly, R. N. 1981. Mars: Hellas Planitia gravity analysis. *Icarus* 45:331-338.

Sleep, N. H., and Phillips. R. J. 1979. An isostatic model for the Tharsis province, Mars. *Geophys. Res. Lett.* 6:803-806.

Sleep, N. H., and Phillips, R. J. 1985. Gravity and lithospheric stress on the terrestrial planets with reference to the Tharsis region of Mars. *J. Geophys. Res.* 90:4469-4489.

Soderblom, L. A., Condit, C. D., West, R. A., Herman, B. M., and Kreidler, R. J. 1974. Martian planetwide crater distributions: Implications for geologic history and surface processes. *Icarus* 22:239-263.

Solomon, S. C. 1978. On volcanism and thermal tectonics on one-plate planets. *Geophys. Res. Lett.* 5:461-464.

Solomon, S. C. 1979. Formation, history and energetics of cores in the terrestrial planets. *Phys. Earth Planet. Int.* 19: 168-182.

Solomon, S. C. 1986. On the early thermal state of the Moon. In *Origin of the Moon*, eds. W. K. Hartmann, R. J. Phillips, and G. J. Taylor (Houston: Lunar and Planetary Institute), pp. 435-452.

Solomon, S. C., and Chaiken, J. 1976. Thermal expansion and thermal stress in the Moon and terrestrial planets: Clues to early thermal history. *Proc. Lunar Sci. Conf.* 7:3229-3243.

Solomon, S. C., and Head, J. W. 1982. Evolution of the Tharsis province

of Mars: The importance of heterogeneous lithospheric thickness and volcanic construction. *J. Geophys. Res.* 87:9755-9774.

Solomon, S. C., and Head, J. W. 1989. Heterogeneities in the thickness of the elastic lithosphere of Mars: Constraints on heat flow and internal dynamics. *J. Geophys. Res.* Submitted.

Spohn, T. 1990. Mantle differentiation and thermal evolution of Mars, Mercury and Venus, *Icarus*, submitted.

Stevenson, D. J. 1980. Lunar symmetry and paleomagnetism. *Nature* 287:520-521.

Stevenson, D. J., Spohn, T. and Schubert, G. 1983. Magnetism and thermal evolution of the terrestrial planets. *Icarus* 54:466-489.

Stevenson, D. J., and Turner, J. S. 1979. Fluid models of mantle convection. In *The Earth, Its Origin, Evolution and Structure*, ed. M. W. McElhinny, (New York: Academic Press), pp. 227-263.

Tanaka, K. L. 1986. The stratigraphy of Mars. *Proc. Lunar Planet. Sci. Conf. XVII. J. Geophys. Res.* 91:E139-E158.

Tanaka, K. L., Isbell, N. K., Scott, D. H., Greeley, R. and Guest, J. E. 1988. The resurfacing history of Mars: A synthesis of digitized, Viking-based geology. *Proc. Lunar Planet. Sci. Conf.* XVIII:665-678.

Taylor, S. R. 1986. The origin of the Moon: Geochemical considerations. In *Origin of the Moon*, Hartmann, W. K., Phillips, R. J. and Taylor G. J., eds.: 125-143.

Thurber, C. H., and Toksöz, M. N. 1978. Martian lithospheric thickness from elastic flexure theory. *Geophys. Res. Lett.* 5:977-980.

Toksöz, M. N. 1979. Planetary seismology and interiors. *Rev. Geophys. Space Phys.* 17:1641-1654.

Toksöz, M. N., and Hsui, A. T. 1978. Thermal history and evolution of

Mars. *Icarus* 32:537-547.

Toksöz, M. N., and Johnston, D. H. 1977. The evolution of the Moon and the terrestrial planets. *The Soviet-American Conference on the Cosmochemistry of the Moon and Planets*, NASA SP-370, pp. 295-327.

Toksöz, M. N., Hsui, A. T., and Johnston, D. H. 1978. Thermal evolutions of the terrestrial planets. *Moon and Planets* 18:281-320.

Tozer, D. C. 1985. Heat transfer and planetary evolution. *Geophys. Surv.* 7:213-246.

Treiman, A. H., Drake M. J., Janssens M.-J., Wold R., and Ebihara, M. 1986. Core formation in the Earth and shergottite parent body (SPB): chemical evidence from basalts. *Geochim. Cosmochim. Acta* 50:1071-1091.

Treiman, A. H., Jones J. H., and Drake M. J. 1987. Core formation in the shergottite parent body and comparison with the Earth. *Proc. Lunar Planet. Sci. Conf. XVII. J. Geophys. Res.* 92:E627-E632.

Turcotte, D. L. 1980. On the thermal evolution of the Earth. *Earth Planet. Sci. Lett.* 48:53-58.

Turcotte, D. L., Cook, F. A., and Willemann, R. J. 1979. Parameterized convection within the Moon and the terrestrial planets. *Proc. Lunar Sci. Conf.* 10:2375-2392.

Turcotte, D. L. and Huang, J. 1990. Implications of crustal fractionation for planetary evolution. *Icarus*. Submitted.

Turcotte, D. L. and Schubert, G. 1982. *Geodynamics* (New York: John Wiley and Sons).

Vogt, P. R. 1974. Volcano height and plate thickness. *Earth Planet. Sci. Lett.* 23:337-348.

Watters, T. R., and Maxwell, T. A. 1983. Crosscutting relations and relative ages of ridges and faults in the Tharsis region of Mars.

Icarus 56:278-298.

Watters, T. R., and Maxwell, T. A. 1986. Orientation, relative age and extent of the Tharsis Plateau ridge system. *J. Geophys. Res.* 91:8113-8125.

Wetherill, G. W. 1974. Problems associated with estimating the relative impact rates on Mars and the Moon. *The Moon* 9:227-231.

Wetherill, G. W. 1985. Occurrence of giant impacts during the growth of the terrestrial planets. *Science* 228:877-879.

Wetherill, G. W. 1986. Accumulation of the terrestrial planets and implications concerning lunar origin. In *Origin of the Moon*, eds. W. K. Hartmann, R. J. Phillips, and G. J. Taylor. (Houston: Lunar and Planetary Institute), pp. 519-550.

Wilhelms, D. E., and Baldwin, R. J. 1988. The relevance of knobby terrain to the Martian dichotomy. In *Abstracts for the MEVTV-LPI Workshop: Early Tectonic and Volcanic Evolution of Mars*. (Houston: Lunar and Planetary Institute), pp. 69-71 (abstract).

Wilhelms, D. E., and Squyres, S. W. 1984. The Martian hemispheric dichotomy may be due to a giant impact. *Nature* 309:138-140.

Willemann, R. J. and Turcotte, D. L. 1982. The role of lithospheric stress in the support of the Tharsis rise. *J. Geophys. Res.* 87:9793-9801.

Wise, D. U., Golombek, M. P., and McGill, G. E. 1979*a*. Tharsis province of Mars: Geologic sequence, geometry, and a deformation mechanism. *Icarus* 38:456-472.

Wise, D. U., Golombek, M. P., and McGill, G. E. 1979*b*. Tectonic evolution of Mars. *J. Geophys. Res.* 84:7934-7939.

Young, R. E., and Schubert, G. 1974. Temperatures inside Mars: Is the

core liquid or solid? *Geophys. Res. Lett.* 1:157-160.

Zebib, A., Schubert, G., Dein, J. L., and Paliwal, R. C. 1983. Character and stability of axisymmetric thermal convection in spheres and spherical shells. *Geophys. Astrophys. Fluid Dynamics* 23:1-42.

Table 1. **Ranges in Properties of the Martian Core Allowed by the Mean Density and Dimensionless Mean Moment of Inertia (after Goettel, 1981).**

Property	Range
Radius	1300 - 1900 km
Fractional Mass	13 - 26 %
Central Pressure	45 - 37 GPa
Density	8900 - 5800 kg m^{-3}

I/MR^2 = 0.365 assumed.

Table 2. Radiogenic Element Abundance Estimates for the Mantles of Mars and Earth

	K (ppm)	Th (ppb)	U (ppb)	K/U	Th/U
MARS*	170	48	16	10^4	3
MARS†	315	56	16	2×10^4	3.5
EARTH‡	257	102.8	25.7	10^4	4

*(Treiman et al., 1986)

†(Laul et al., 1986)

‡(Turcotte and Schubert, 1982)

Table 3. **Parameter Values for Three-Dimensional Spherical Convection Models of the Martian Mantle**

Outer Radius	3200 km
Inner Radius	1762 km
Density	3450 kg m^{-3}
Core Mass	1490 x 10^{20} kg
Kinematic Viscosity	10^{18} m^2 s^{-1}
Thermal Diffusivity	10^{-6} m^2 s^{-1}
Specific Heat at Constant Pressure	1.2 kJ kg^{-1} K^{-1}
Thermal Expansivity	2 x 10^{-5} K^{-1}
Temperature Difference Across the Mantle	800 K
Internal Heating Rate (94% from below)	1.5 x 10^{-13} W kg^{-1}
Internal Heating Rate (20% from below)	5.3 x 10^{-12} W kg^{-1}

Figure Captions

Figure 1. Core density ρ_c, mantle density ρ_m and fractional core mass vs. normalized core radius x for a two-layer model of Mars consistent with the mean density (3393 kg m^{-3}) and dimensionless moment of inertia (0.365). The curves are simultaneous solutions of the equations 3933 kg $m^{-3} = \rho_m + (\rho_c - \rho_m)x^3$ and $(0.365)(3933)(2.5)$ kg $m^{-3} = \rho_m + (\rho_c - \rho_m)x^5$.

Figure 2. Model accretional temperature profiles for Mars (after Coradini et al., 1983). The calculations are based on a 100 Myr accretion timescale and the assumption that 30% of the impact kinetic energy is retained as heat in the growing planet. The dashed curve is a model solidus temperature profile.

Figure 3. Heat flow from the mantle versus time for two models of Martian thermal history. Details of the models are given in Stevenson et al. (1983). The models have initial core sulfur concentrations x_S of 10 and 25 weight percent, respectively.

Figure 4. The decrease of characteristic mantle temperature with time in the Martian thermal history models of Figure 3.

Figure 5. Thickening of the Martian lithosphere with time in the cooling models of Figure 3.

Figure 6. Core heat flux as a function of time in the Martian thermal evolution models of Figure 3. The horizontal line marks the conductive heat flux along an adiabat in the liquid outer core. The sharp bend in the curve for the model with $x_S = 0.10$ denotes the onset of inner core solidification.

Figure 7. Contours of fractional inner core radius as a function of present mantle kinematic viscosity and initial weight percent sulfur (x_S)

in the core (after Schubert and Spohn, 1990).

Figure 8. Fractional inner core radius versus time for model cooling histories of Mars with three different initial sulfur concentrations in the core (after Schubert and Spohn, 1990).

Figure 9. Normalized magnetic dipole moment versus time for the models of Figure 3. Dipole moment is normalized with respect to the value of the present moment in the model with $x_S = 0.10$. Computed following the method presented in Schubert and Spohn (1990).

Figure 10. Dependence of the mean mantle temperature T on time t for several values of the crustal fractionation parameter χ.

Figure 11. Thickness of the crust D_c versus time t for a number of values of the crustal fractionation parameter χ. The crustal thickness for a fully differentiated Mars is $D_{co} = 154$ km.

Figure 12. Dependence of the volumetric flux of Martian volcanism V_v on time t for several values of the crustal fractionation parameter χ.

Figure 13. Thickness of the Martian lithosphere D_L versus time t for several values of the crustal fractionation parameter χ.

Figure 14. Dependence of the mantle heat flux Q_s on time t for different values of the crustal fractionation parameter χ.

Figure 15. Radial expansion (contraction) $\delta R/R$ as a function of time t for several values of the crustal fractionation parameter χ.

Figure 16. Contours of radial velocity at mid-depth in the Martian mantle in numerical models of three-dimensional mantle convection with (a) 20% and (b) 94% heating from below. The projection is an equal-area projection extending 360° in longitude and over all latitudes. Model parameter values are listed in Table 3 (after Schubert et al., 1990).

Solid contours indicate radially outward motion, dashed contours denote radially inward motion.

Figure 17. Meridional cross-sections of temperature in the numerical models of Figure 13 for (a) 20% and (b) 94% heating from below.

Figure 18. (a) and (b) are similar to Figures 16 and 17 but for a small Martian core of radius 0.2 times the radius of Mars. In the model 90% of the heating is from below.

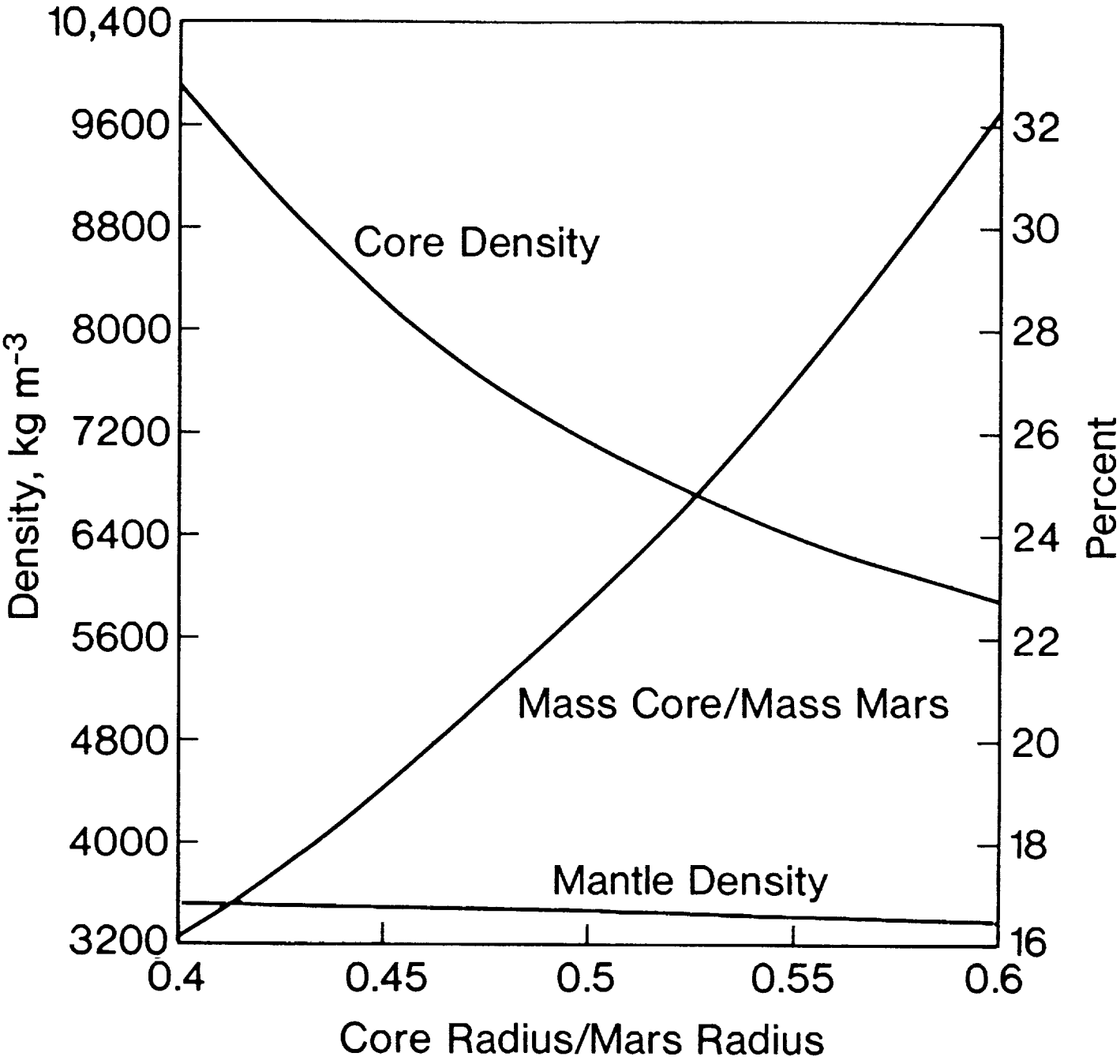
10,400
9600
8800
8000
7200
6400
5600
4800
4000
3200
Density, kg m-3
Core Density
Mass Core/Mass Mars
Mantle Density
32
30
28
26
24
22
20
18
16
Percent
0.4
0.45
0.5
0.55
0.6
Core Radius/Mars Radius

Figure 1.

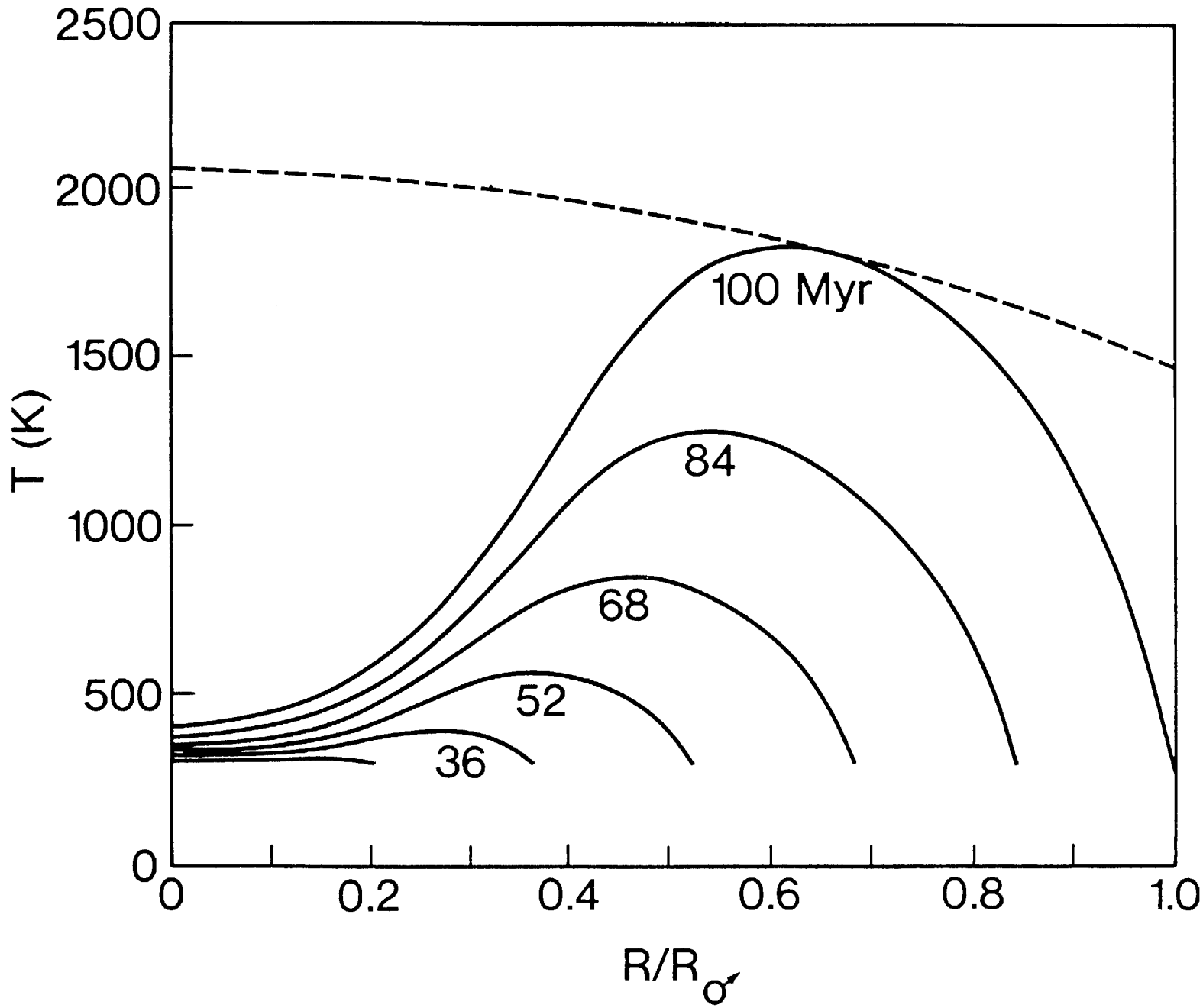

Figure 2.

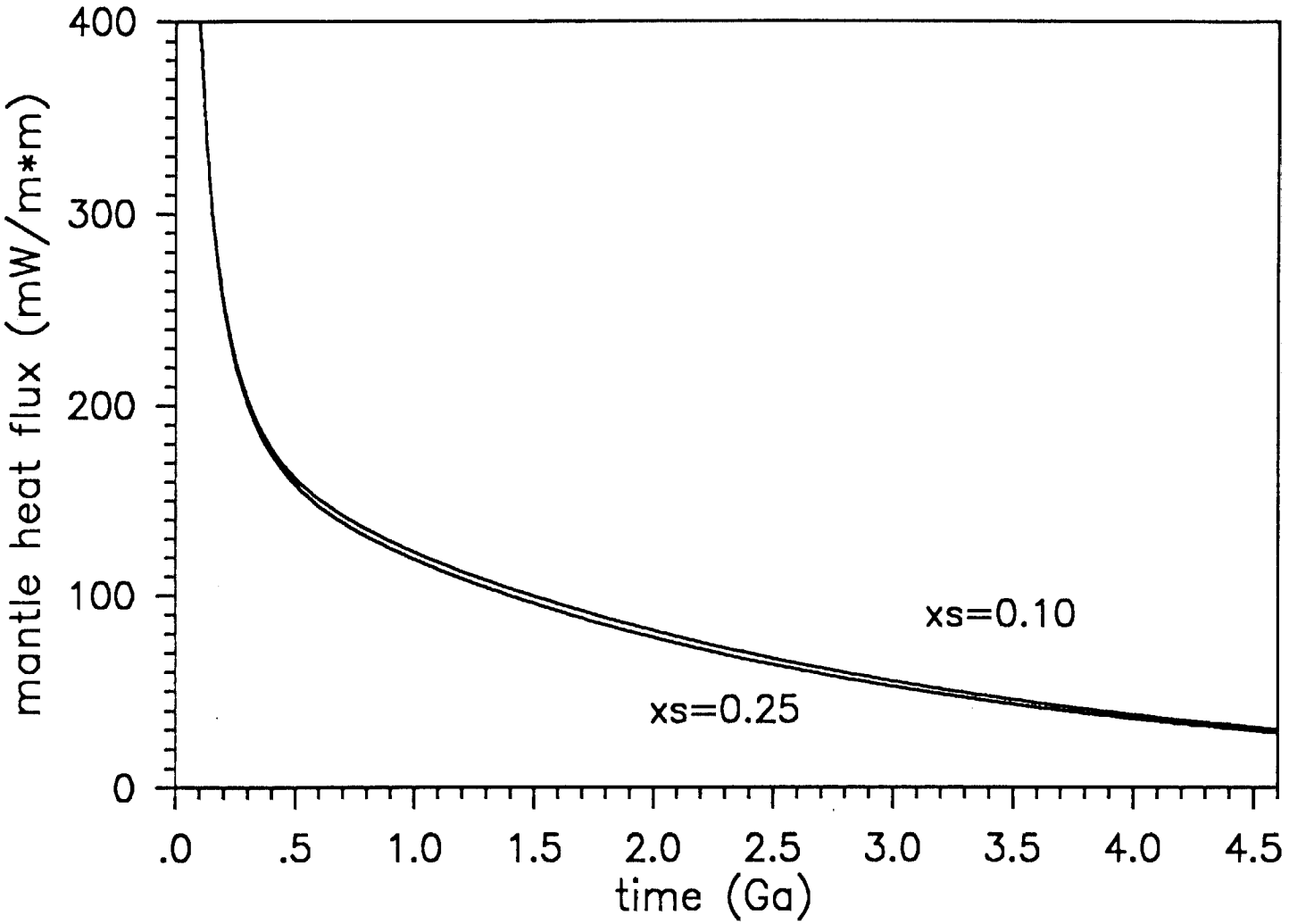
400
300
200
100
0
mantle heat flux (mW/m*m)
xs=0.10
xs=0.25
.0
.5
1.0
1.5
2.0
2.5
3.0
3.5
4.0
4.5
time (Ga)

Figure 3.

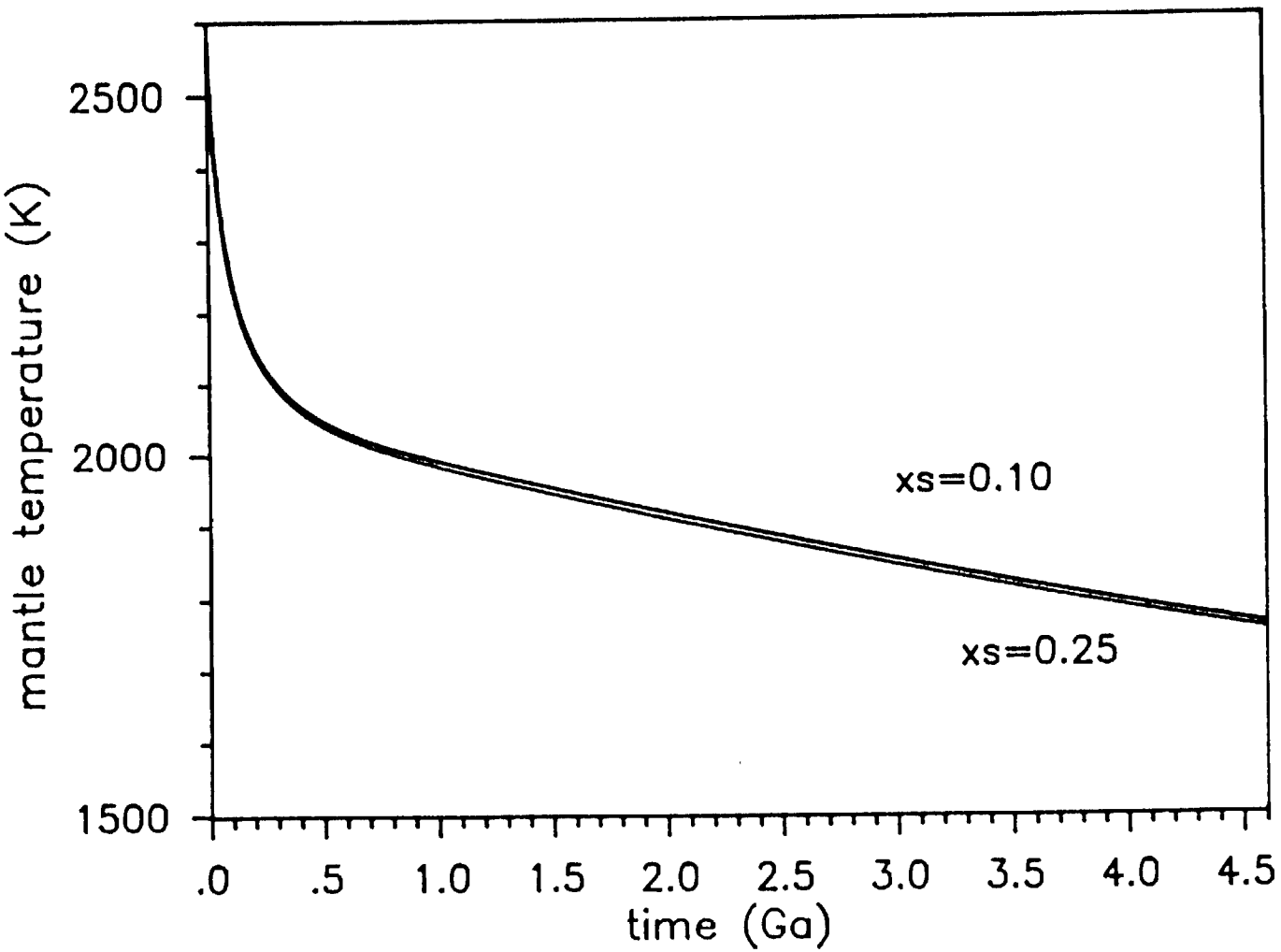
mantle temperature (K)
2500
2000
1500
xs=0.10
xs=0.25
.0
.5
1.0
1.5
2.0
2.5
3.0
3.5
4.0
4.5
time (Ga)

Figure 4.

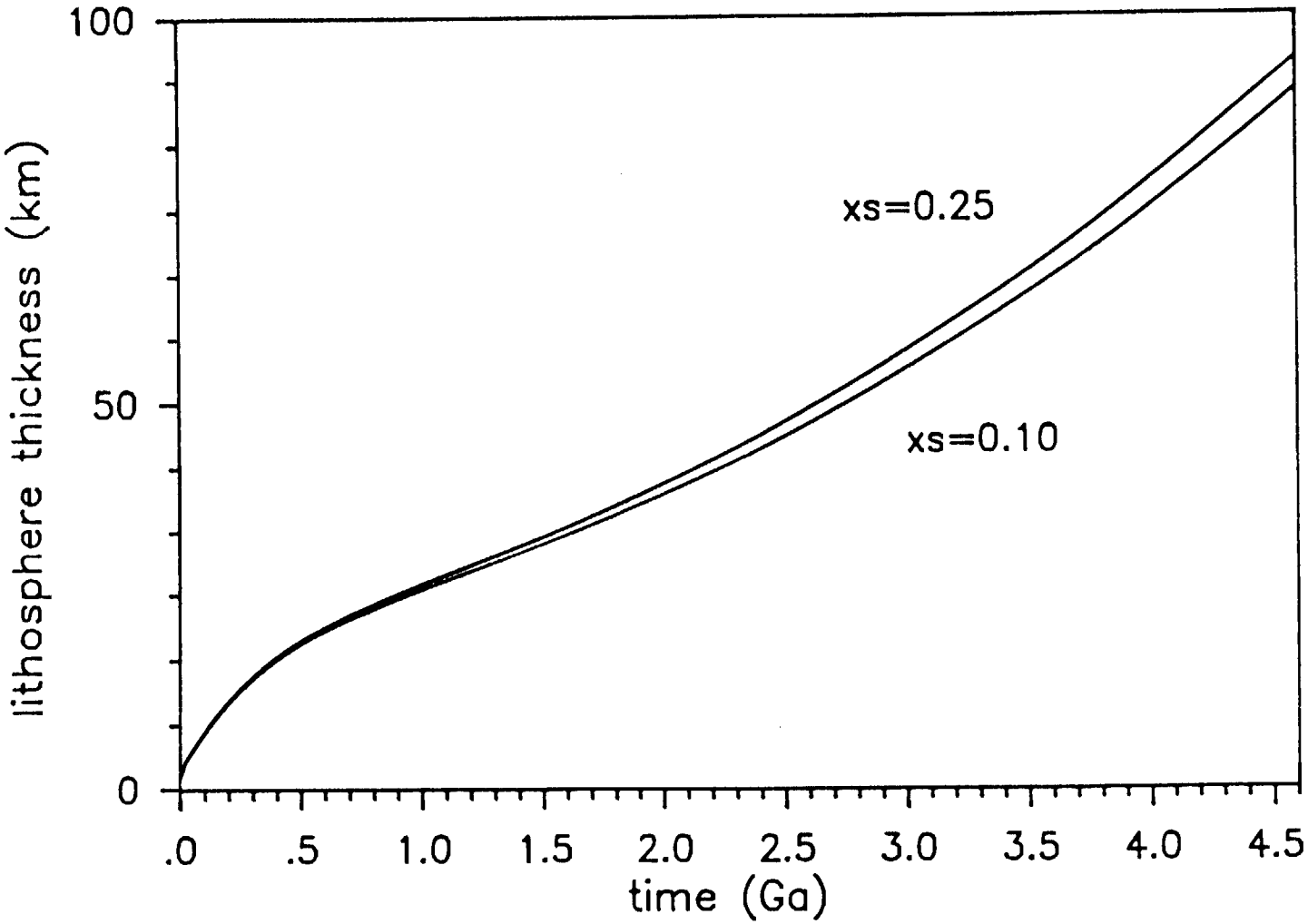
100
50
0
lithosphere thickness (km)
xs=0.25
xs=0.10
.0
.5
1.0
1.5
2.0
2.5
3.0
3.5
4.0
4.5
time (Ga)

Figure 5.

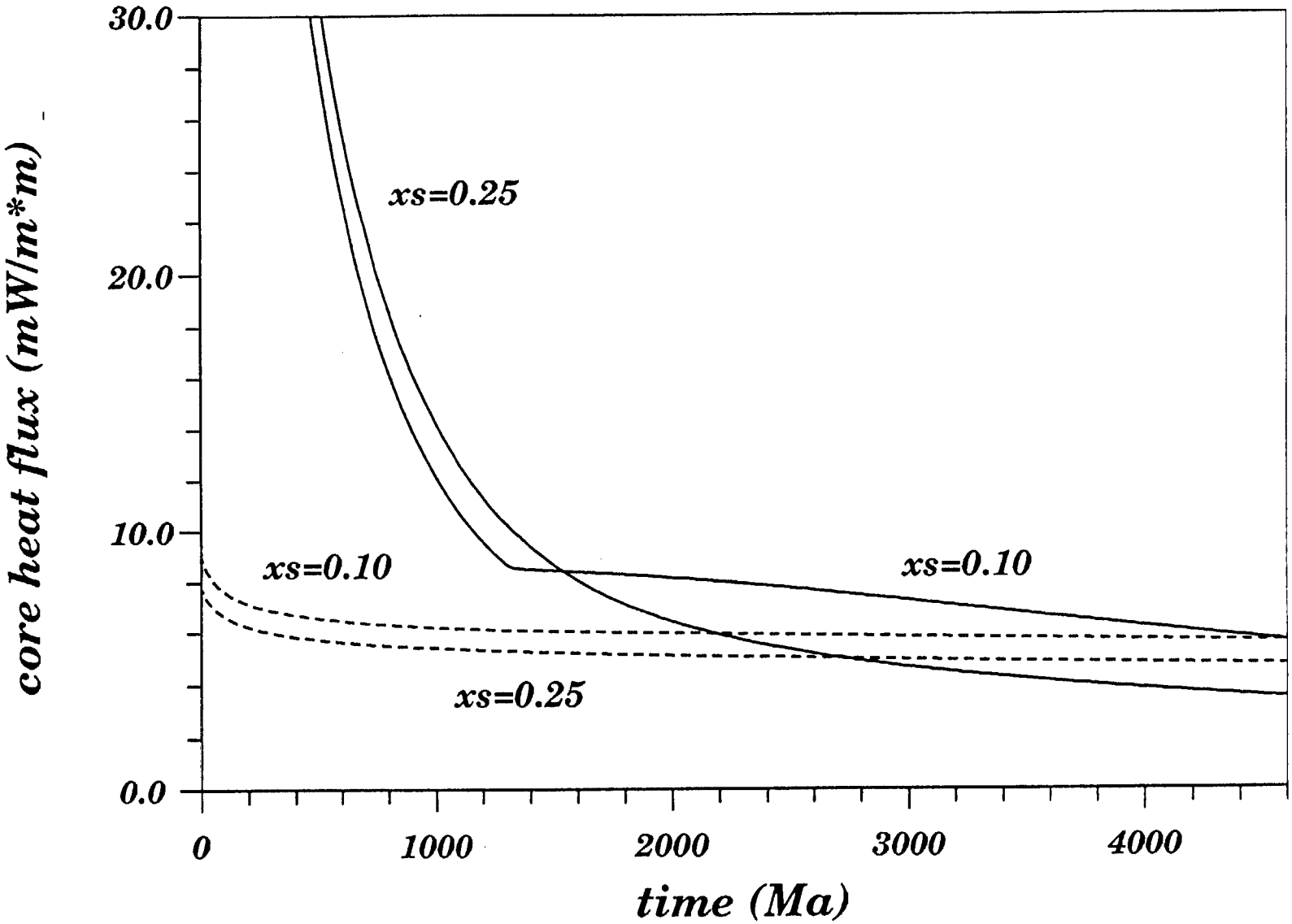
30.0
20.0
10.0
0.0
core heat flux (mW/m*m)
xs=0.25
xs=0.10
xs=0.10
xs=0.25
0
1000
2000
3000
4000
time (Ma)

Figure 6.

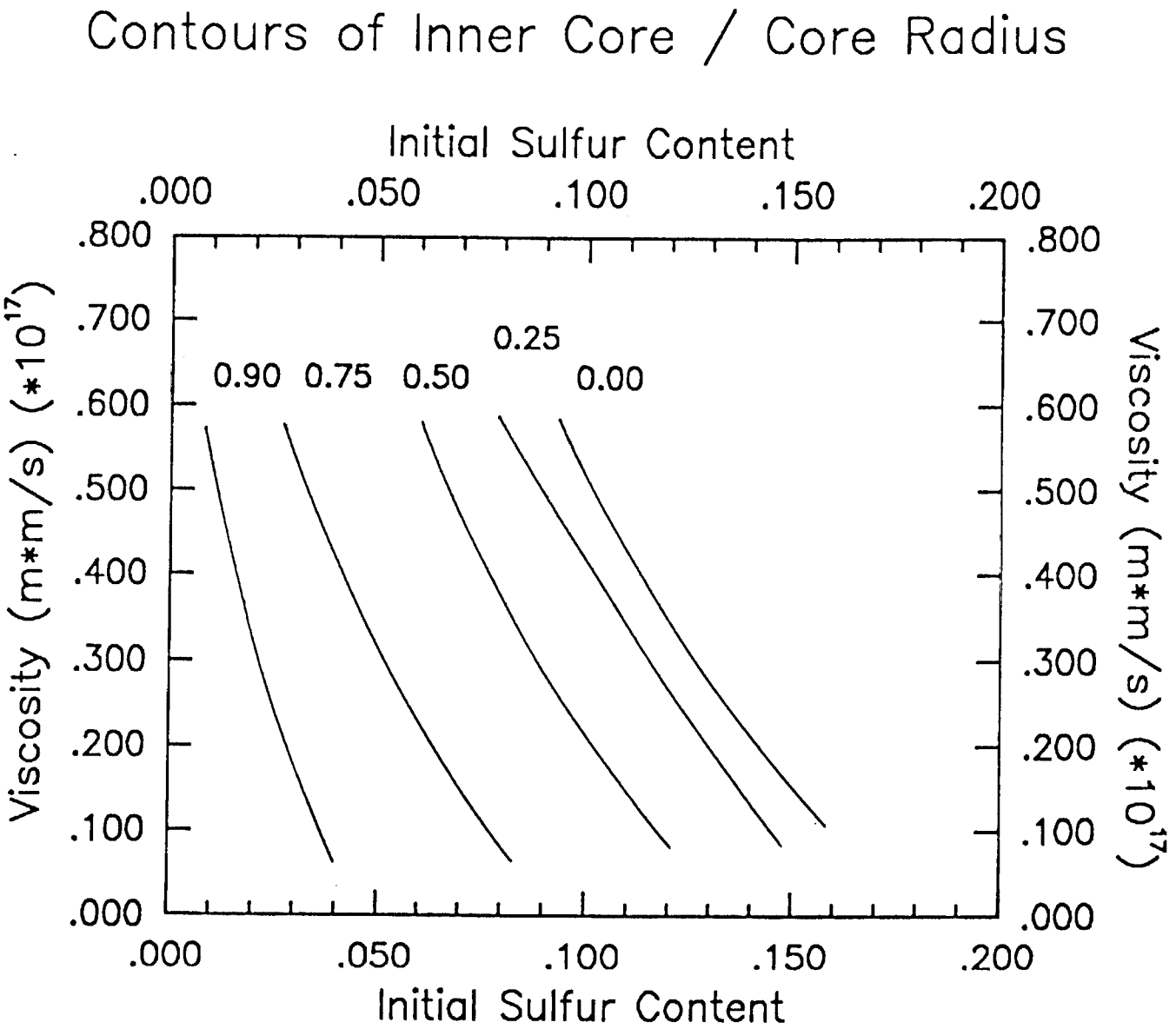
Contours of Inner Core / Core Radius
Initial Sulfur Content
.000
.050
.100
.150
.200
.800
.700
.600
.500
.400
.300
.200
.100
.000
Viscosity (m*m/s) (*10^17)
0.90
0.75
0.50
0.25
0.00
Initial Sulfur Content
Viscosity (m*m/s) (*10^17)

Figure 7.

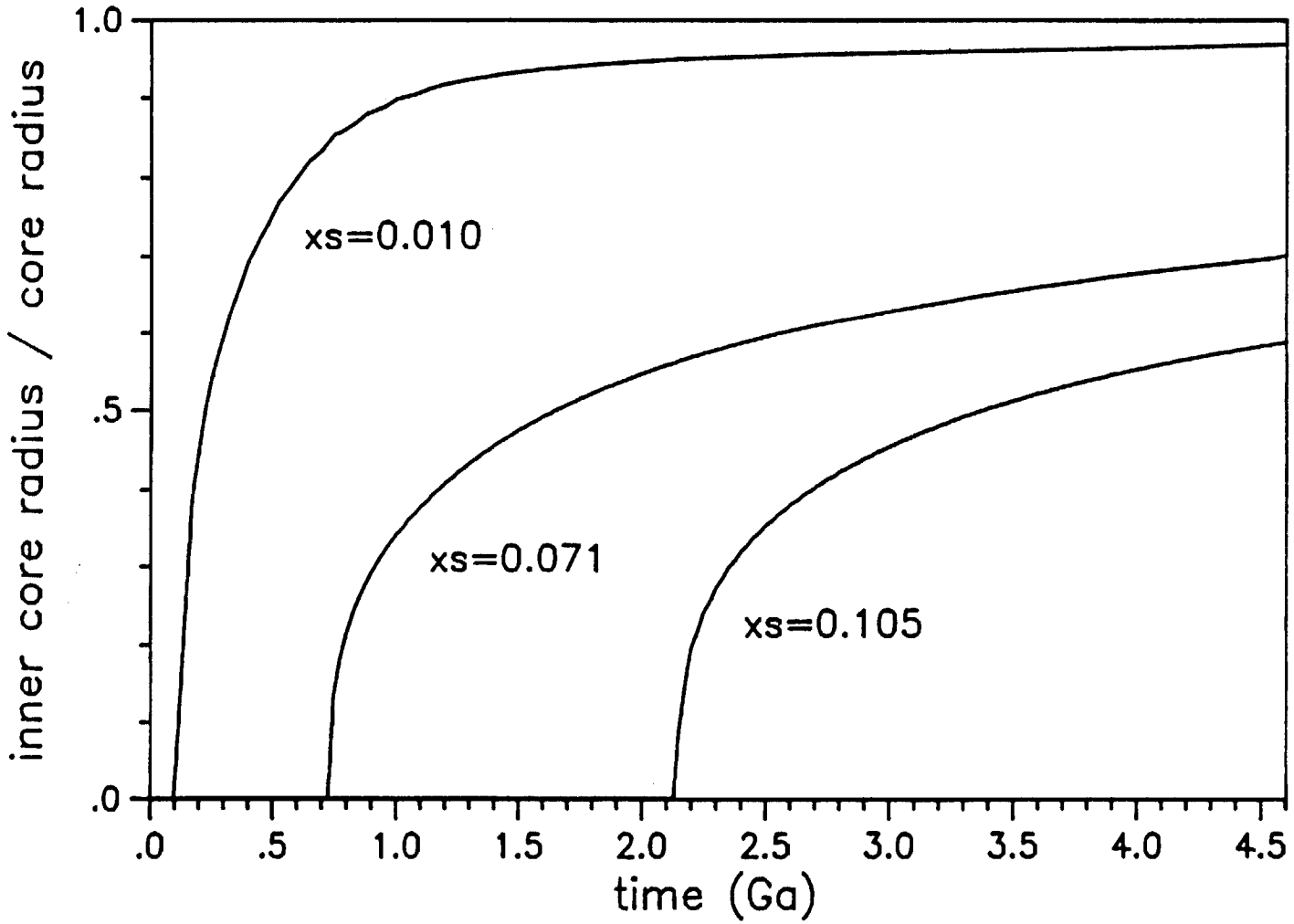
1.0
.5
.0
inner core radius / core radius
xs=0.010
xs=0.071
xs=0.105
.0
.5
1.0
1.5
2.0
2.5
3.0
3.5
4.0
4.5
time (Ga)

Figure 8.

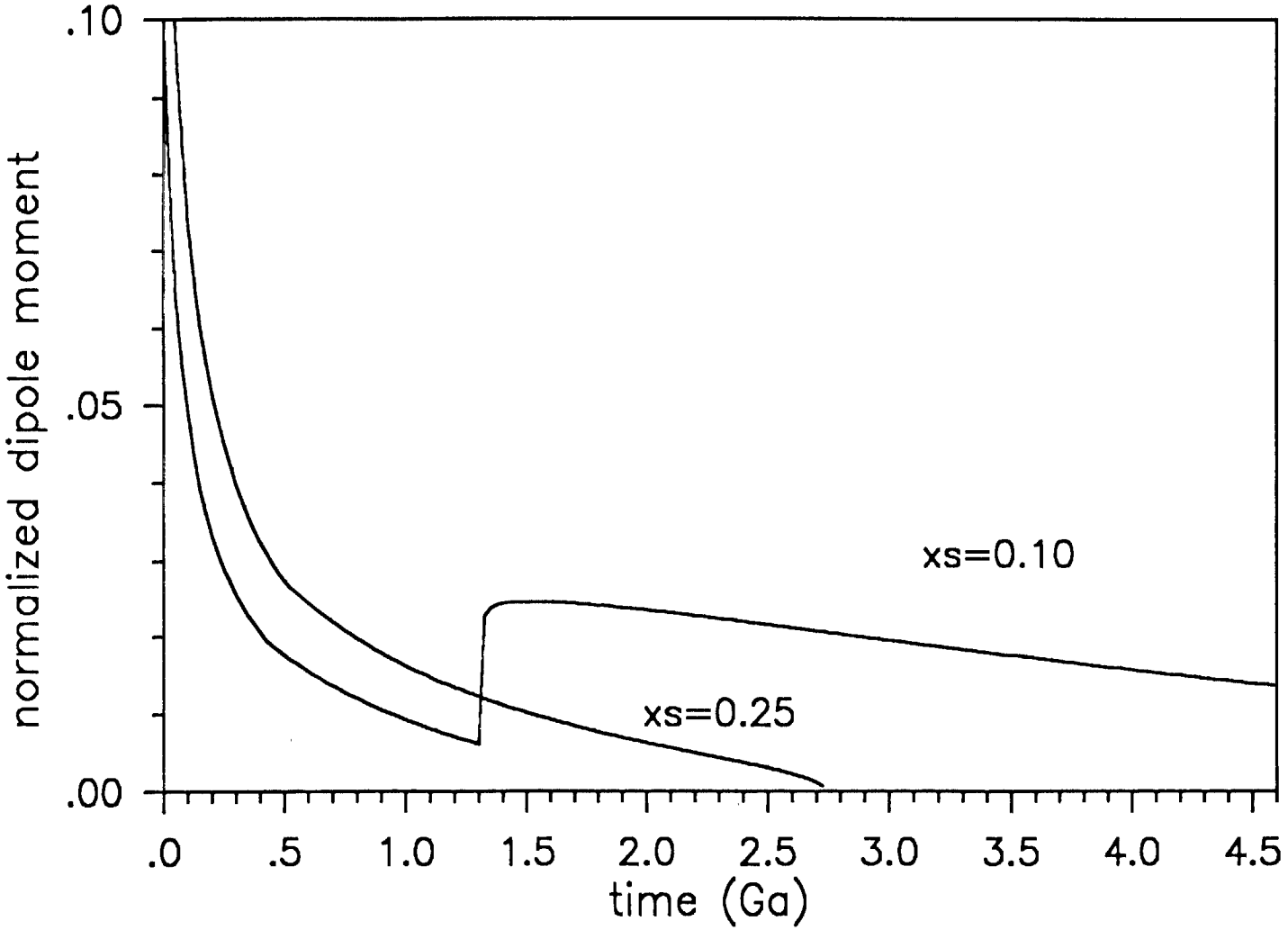
.10
.05
.00
normalized dipole moment
xs=0.10
xs=0.25
.0
.5
1.0
1.5
2.0
2.5
3.0
3.5
4.0
4.5
time (Ga)

Figure 9.

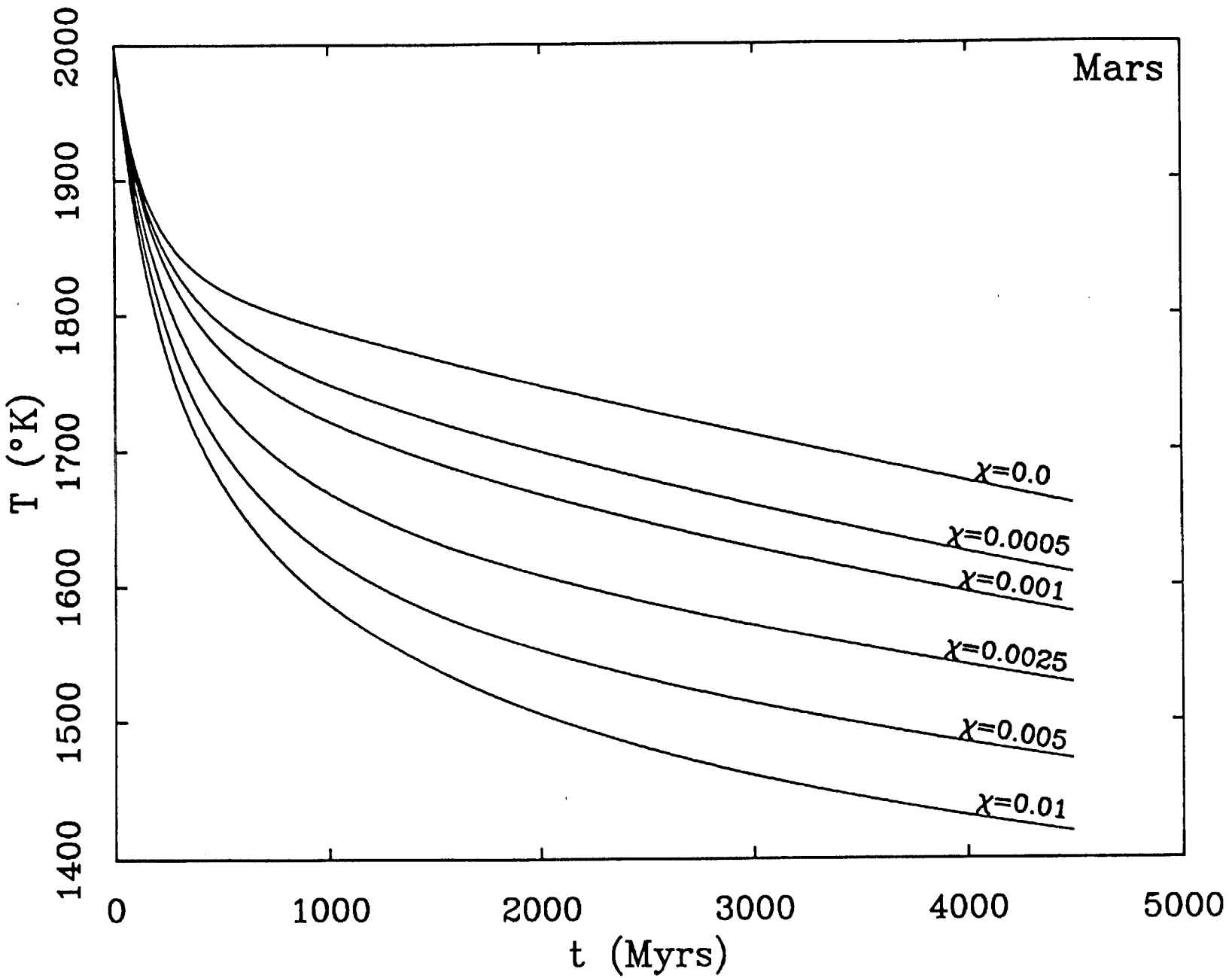
Mars
T (°K)
1400
1500
1600
1700
1800
1900
2000
0
1000
2000
3000
4000
5000
t (Myrs)
χ=0.0
χ=0.0005
χ=0.001
χ=0.0025
χ=0.005
χ=0.01

Figure 10.

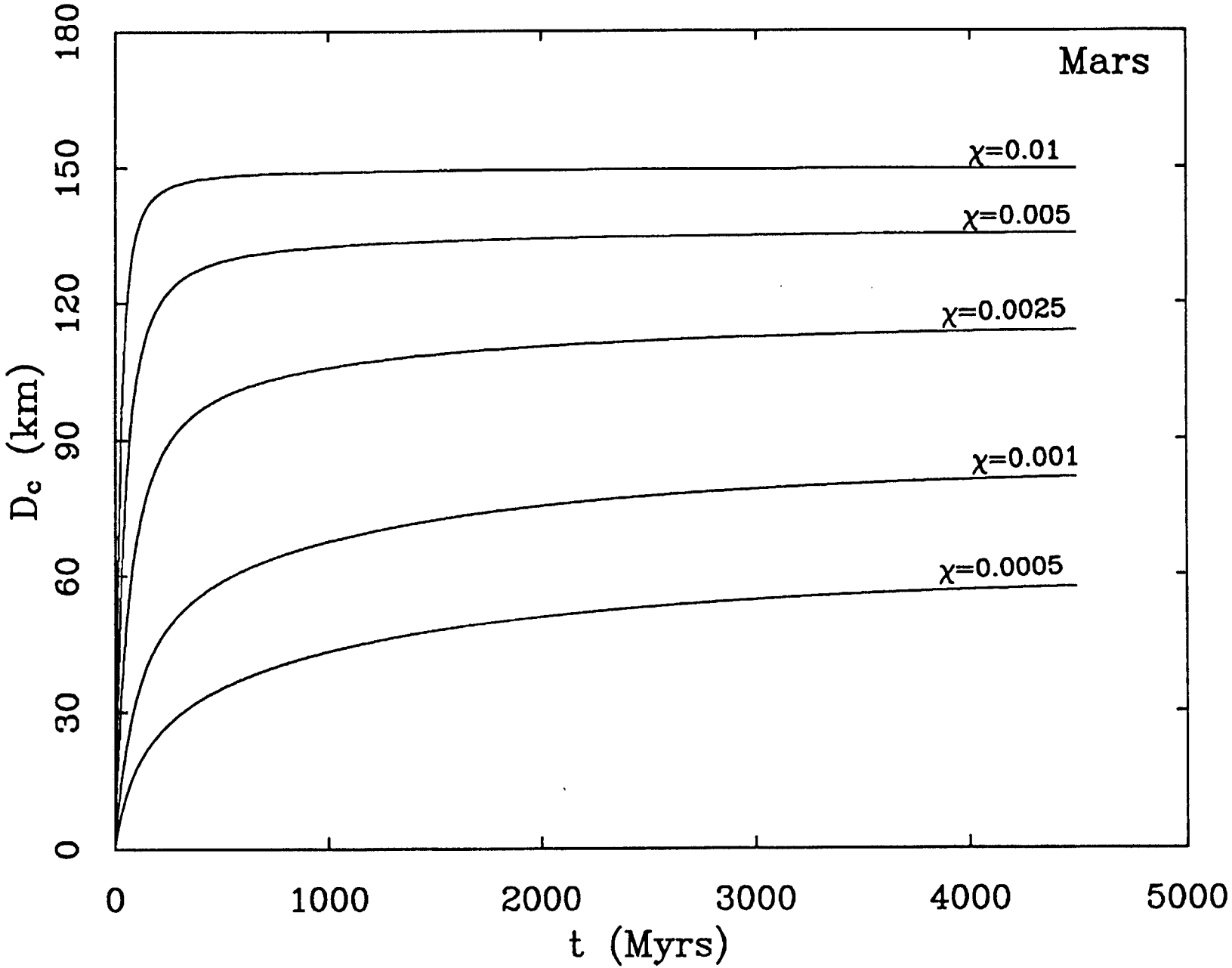
Mars
χ=0.01
χ=0.005
χ=0.0025
χ=0.001
χ=0.0005
D_c (km)
0
30
60
90
120
150
180
0
1000
2000
3000
4000
5000
t (Myrs)

Figure 11.

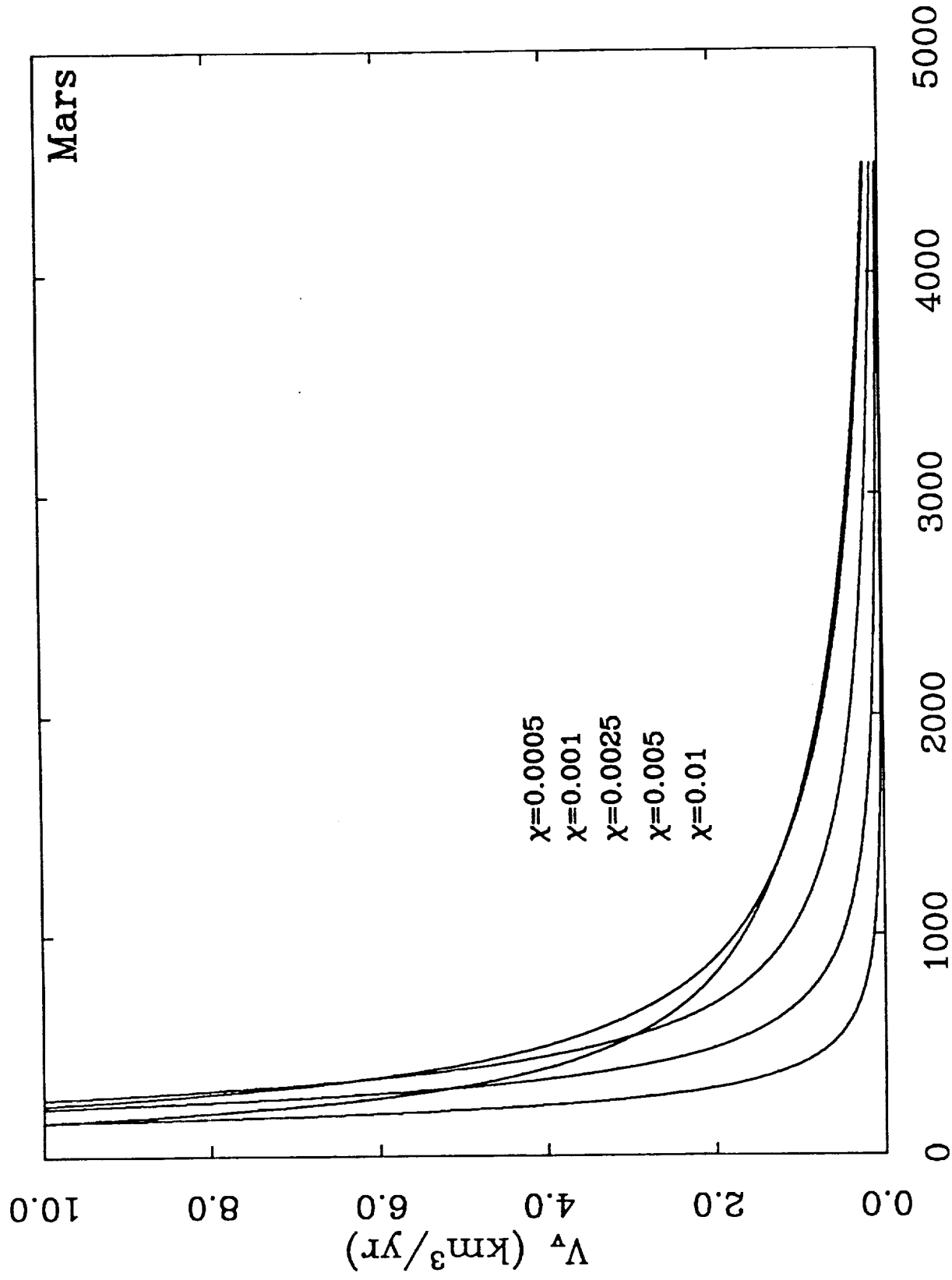
Mars
χ=0.0005
χ=0.001
χ=0.0025
χ=0.005
χ=0.01
V∞ (km³/yr)
t (Myrs)
0.0
2.0
4.0
6.0
8.0
10.0
0
1000
2000
3000
4000
5000

Figure 12.

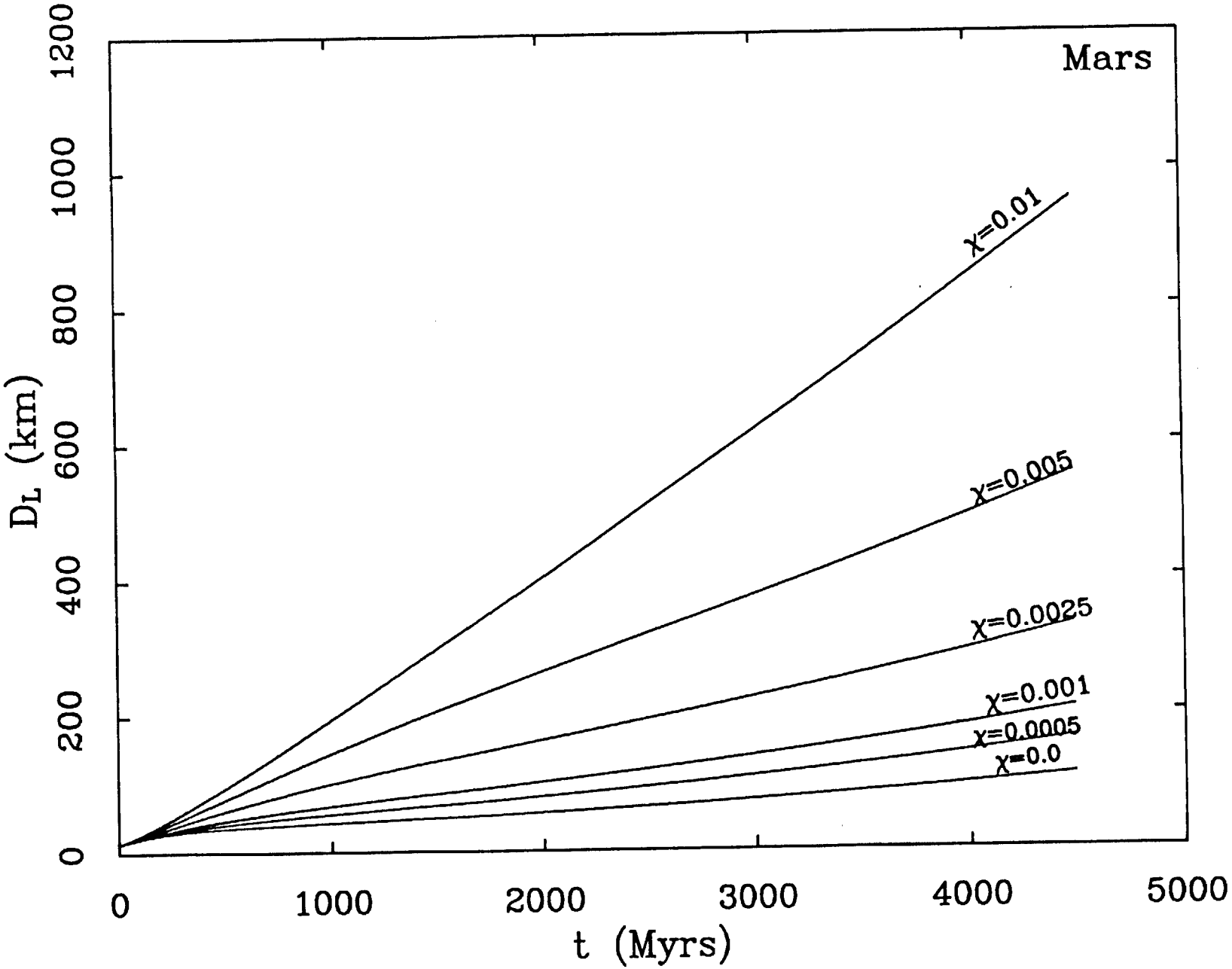
Mars
D_L (km)
0
200
400
600
800
1000
1200
0
1000
2000
3000
4000
5000
t (Myrs)
χ=0.01
χ=0.005
χ=0.0025
χ=0.001
χ=0.0005
χ=0.0

Figure 13.

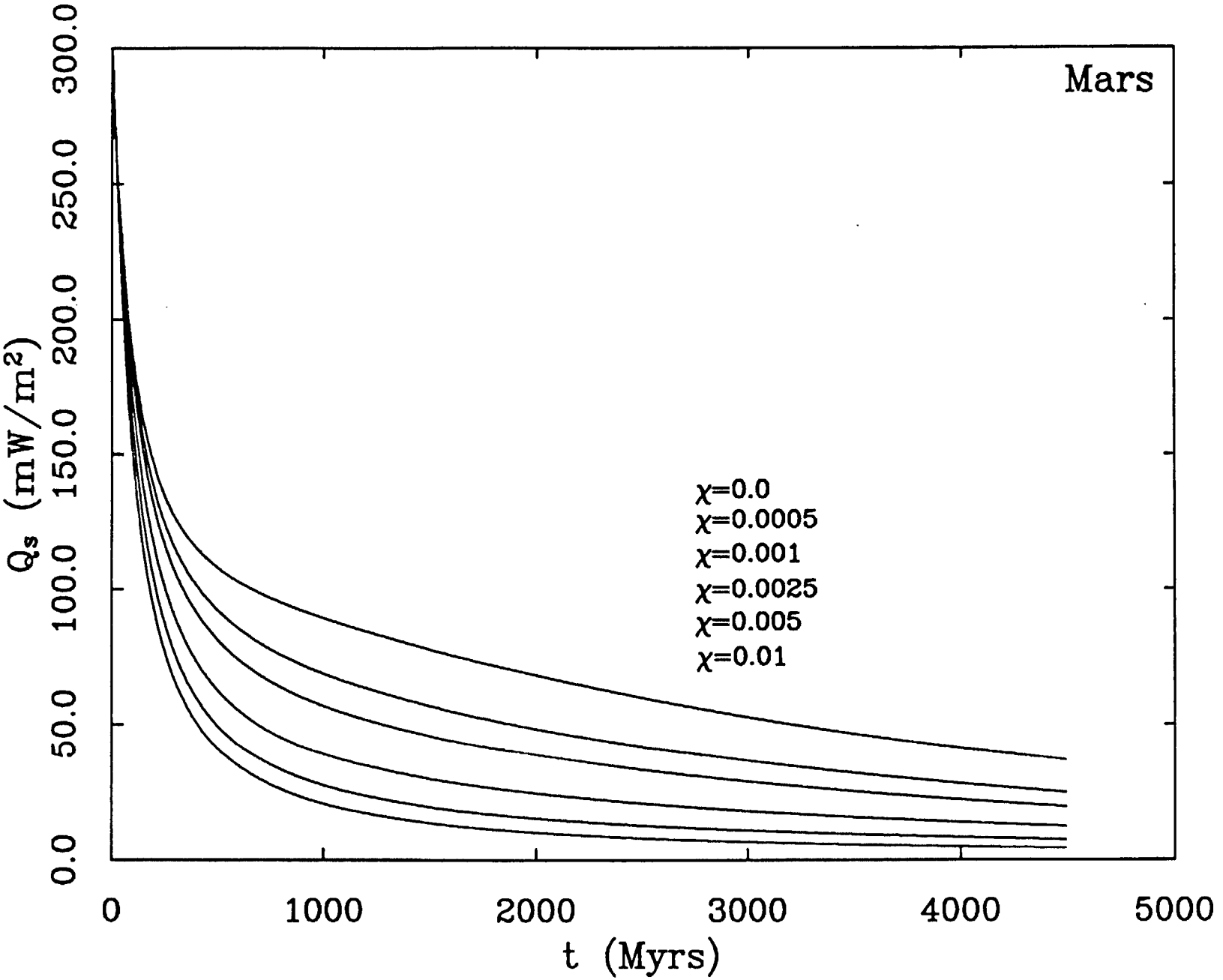
Mars
Q_s (mW/m^2)
0.0
50.0
100.0
150.0
200.0
250.0
300.0
0
1000
2000
3000
4000
5000
t (Myrs)
χ=0.0
χ=0.0005
χ=0.001
χ=0.0025
χ=0.005
χ=0.01

Figure 14.

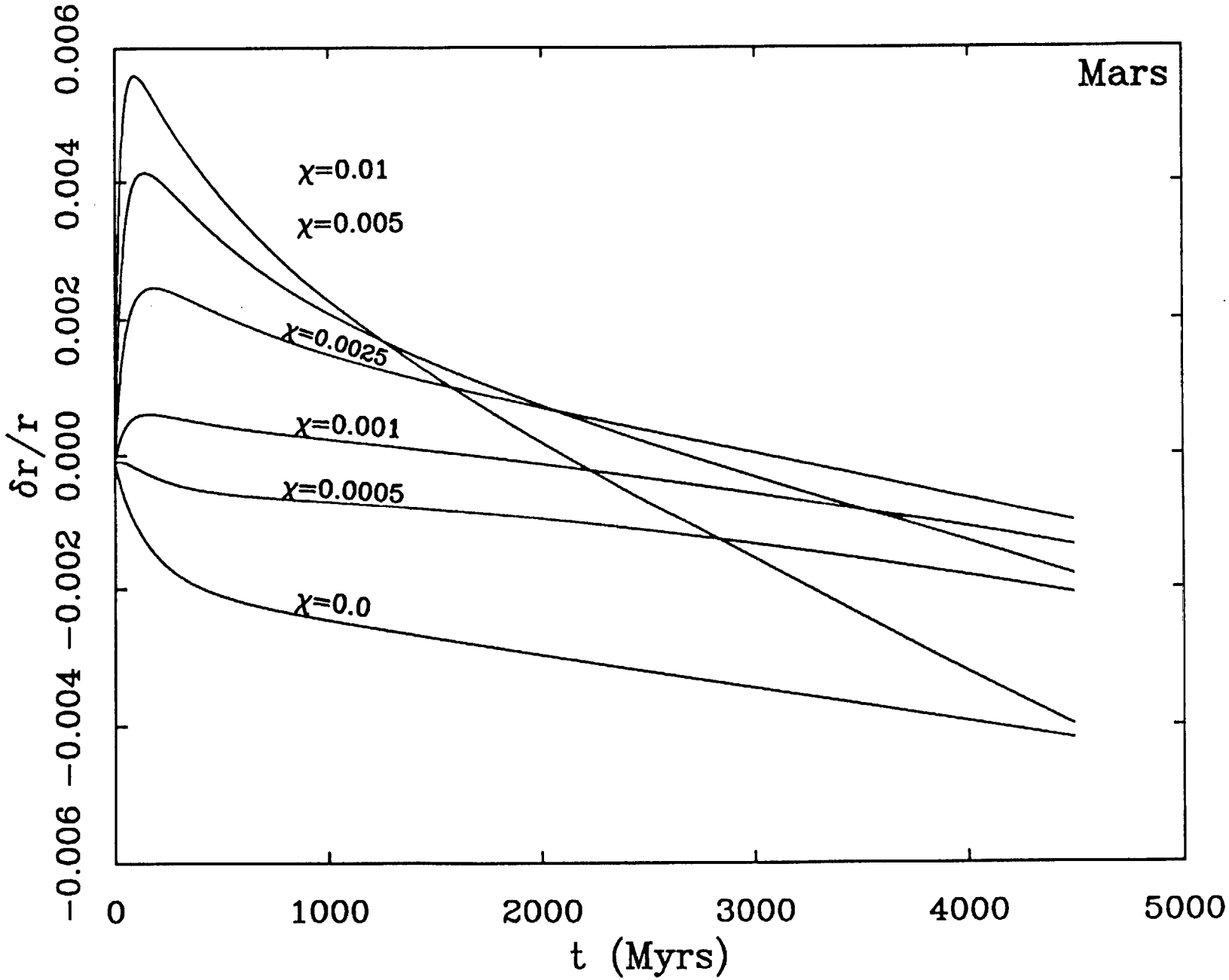
Mars
χ=0.01
χ=0.005
χ=0.0025
χ=0.001
χ=0.0005
χ=0.0
δr/r
0.006
0.004
0.002
0.000
−0.002
−0.004
−0.006
0
1000
2000
3000
4000
5000
t (Myrs)

Figure 15.

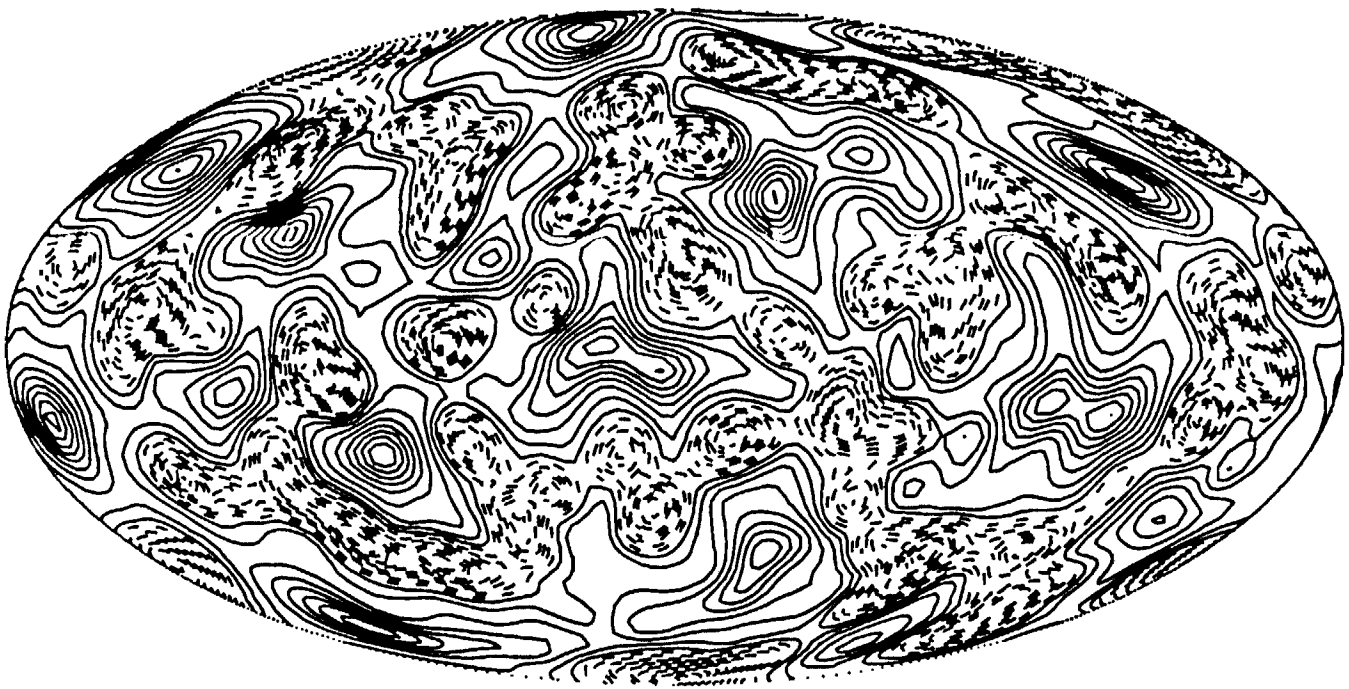

Figure 16a.

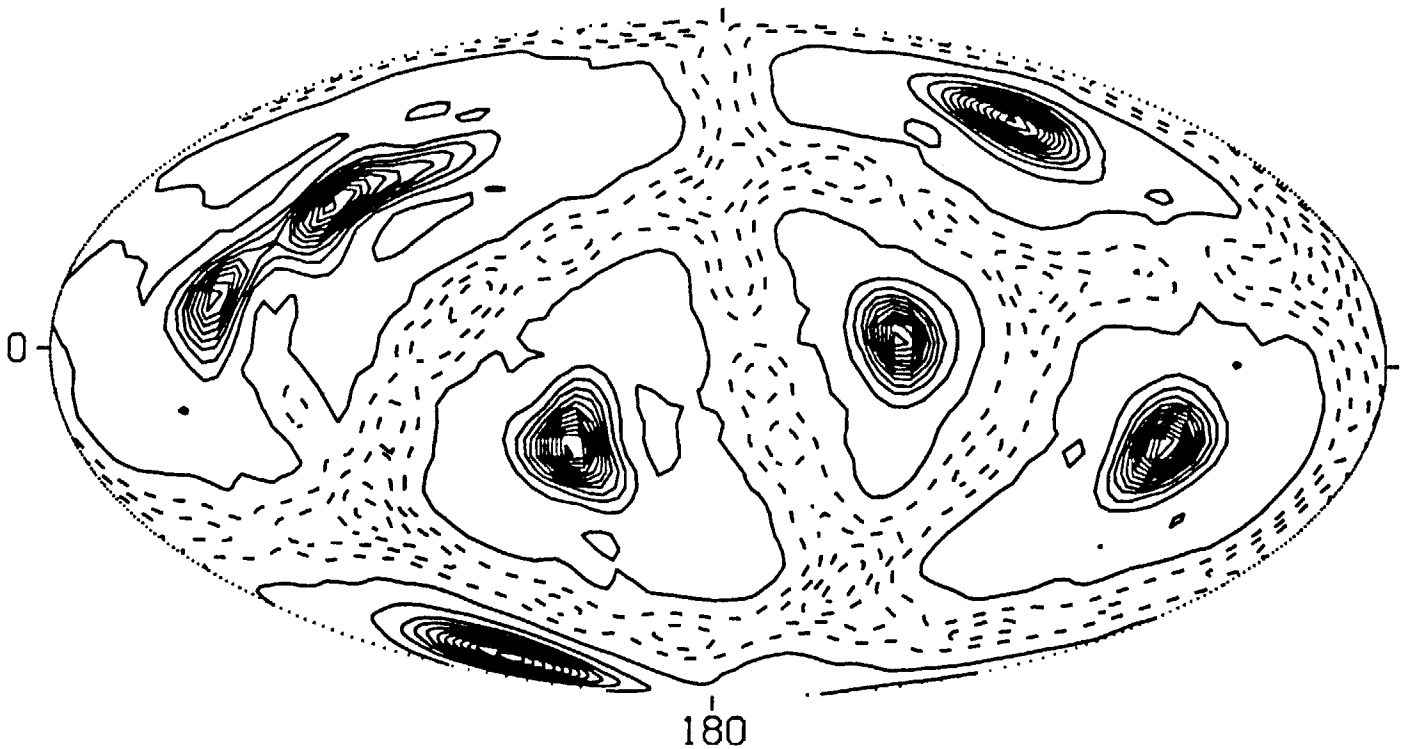

Figure 16b.

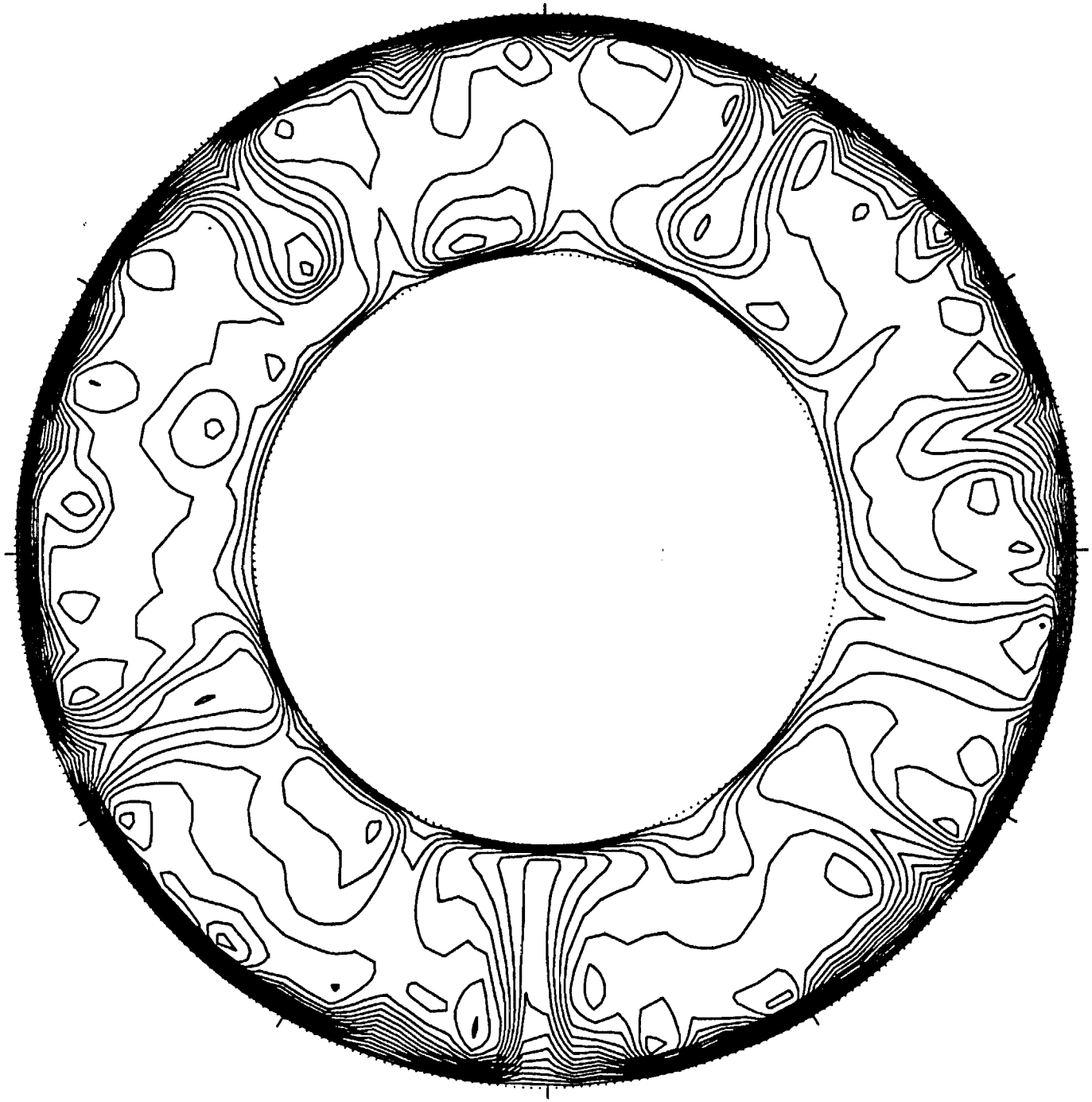

Figure 17a.

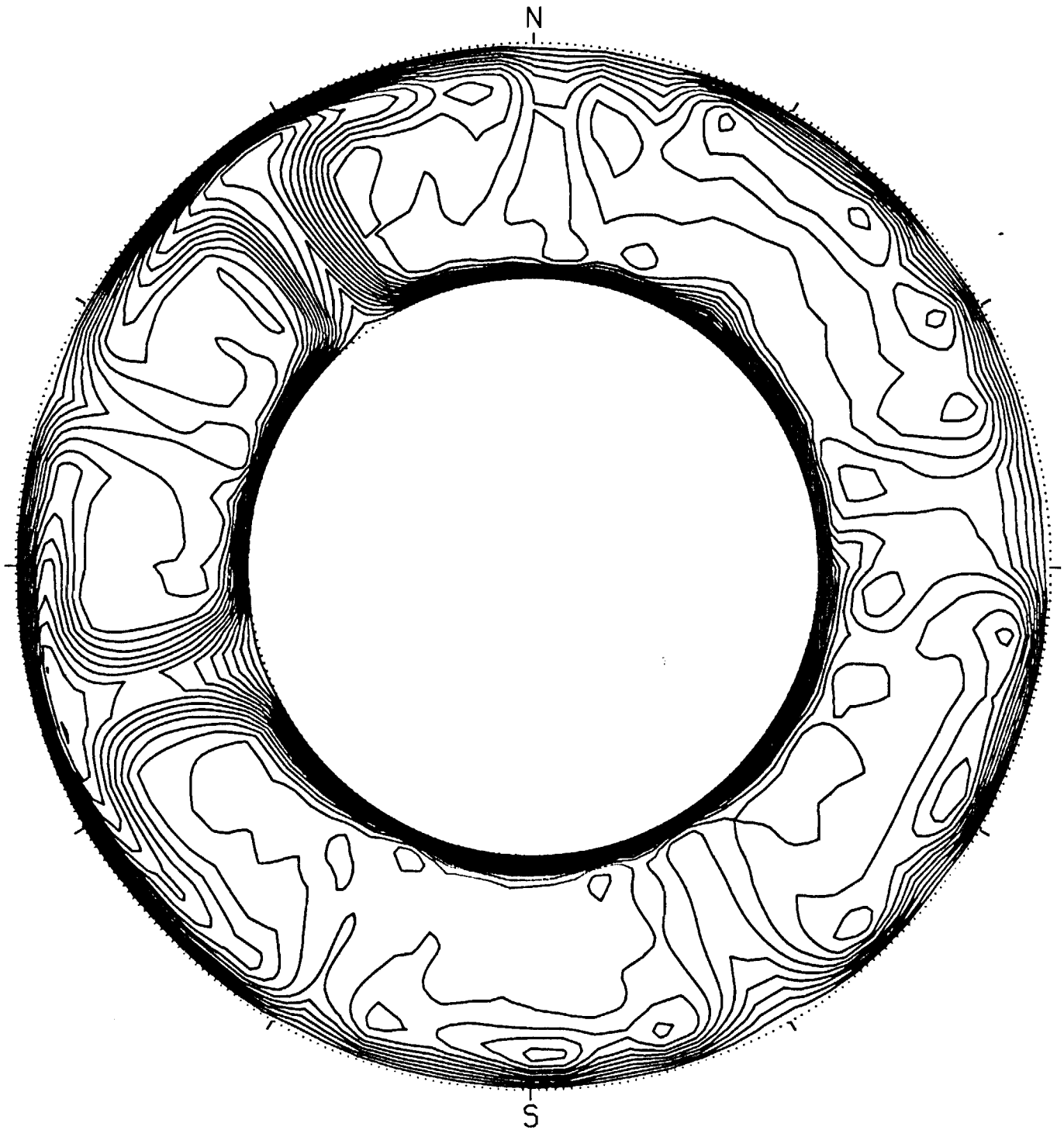

Figure 17b.

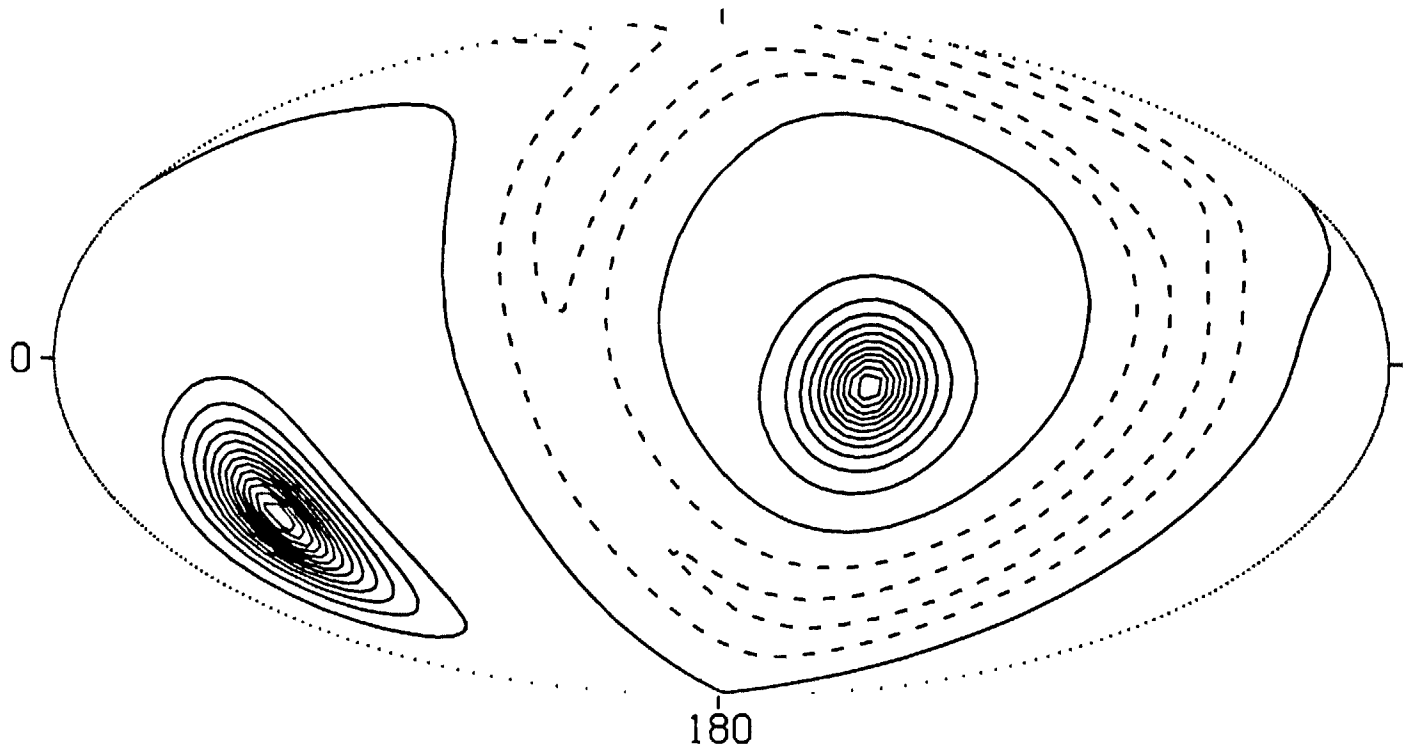

Figure 18a.

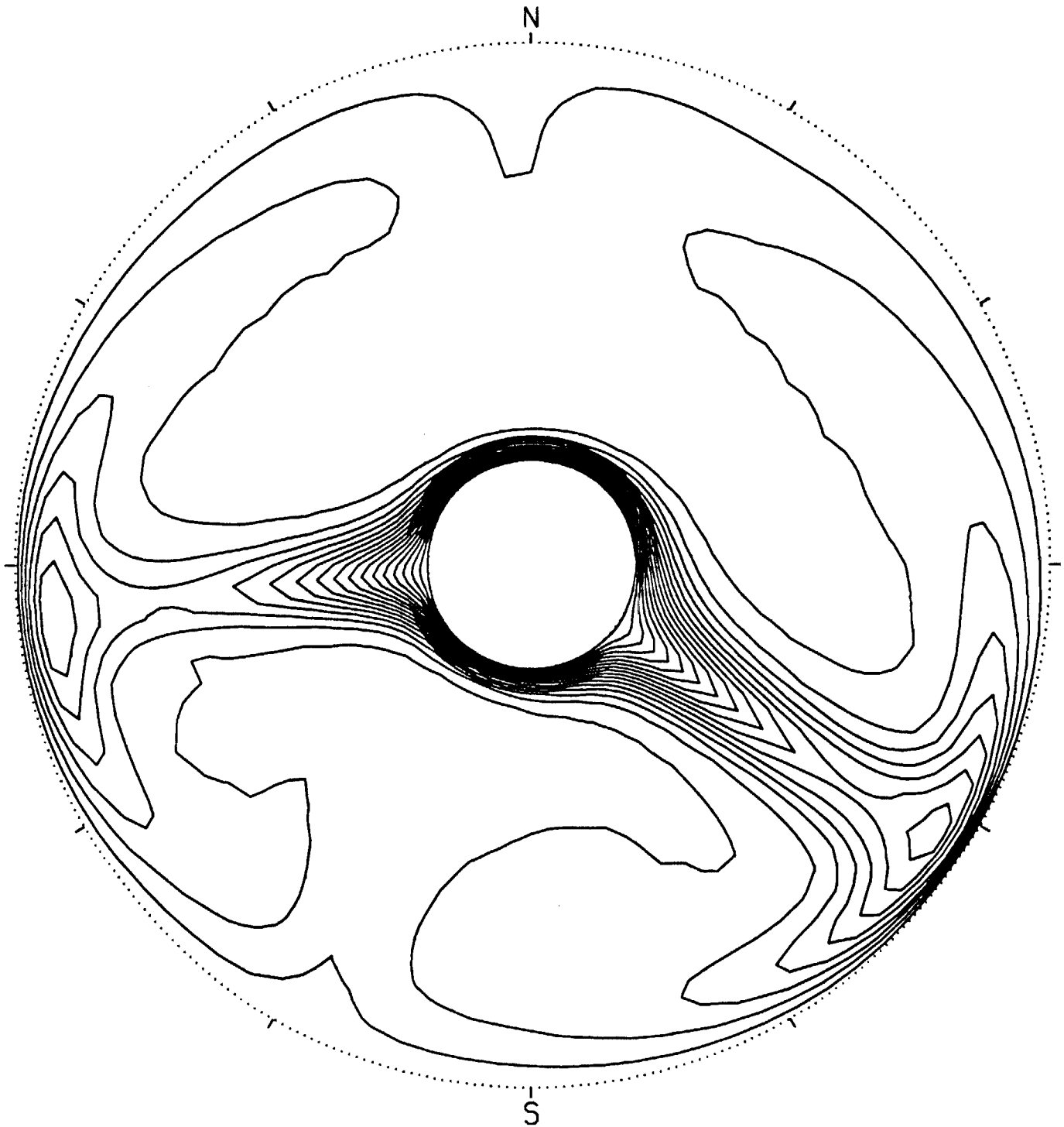

Figure 18b.